

Synthesis and Structural Characterization of Porphyrinic Eneidyne: Geometric and Electronic Effects on Thermal and Photochemical Reactivity

Tilak Chandra, Brian J. Kraft, John C. Huffman, and Jeffrey M. Zaleski*

Department of Chemistry and Molecular Structure Center, Indiana University, Bloomington, Indiana 47405-7102

Received January 28, 2003

We report the preparation of [5,10,15,20-tetraphenyl-2,3,7,8,12,13,17,18-octakis(phenylethynyl)porphinato] complexes of Ni(II), H₂, Zn(II), Mg(II), and Cu(II), as well as select trimethylsilanylethynyl derivatives. The X-ray structures of the octakis(phenylethynyl) compounds show systematic deviations from planarity (Ni(II), 0.2851 Å; Zn(II), 0.0304 Å) as a function of the central cation. These geometric distortions are reflected in bathochromic shifts of the Soret and Q bands (Ni(II), 497, 604, and 650 nm; Mg(II), 515, 595, 642, and 705 nm) which loosely correlate with increasing planarity of the structure. Similarly, vibrational modes involving the octasubstituted porphyrin core exhibit shifts to lower frequency as a function of increasing planarity in the solution-state resonance Raman spectra ($\lambda_{\text{exc}} = 501.7$ nm) of these compounds. Analogous trends are also observed in their solid-state electronic and resonance Raman spectra, indicating that the structural distortions within the octakis(phenylethynyl) series are preserved in solution. Comparison of the saddle distortion of the octasubstituted Ni(II) compound with the ruffle/saddle distortions of the pentakis and hexakis Ni(II) derivatives reveals some influence of asymmetric periphery substitution on geometric structure. These Ni(II) derivatives also exhibit systematic red shifts in their electronic spectra as a function of the number of conjugated alkyne units (~ 13 nm/alkyne), revealing participation of the enediyne units in the electronic ground and excited states. The solid-state Bergman cyclization temperatures of the phenylethynyl compounds vary markedly as a function of planarity, and correlate loosely with alkyne termini separation (Ni(PA)₈, 4.00 Å, 281 °C; MgP(PA)₈, 3.77 Å, 244 °C). In solution, both thermal and photochemical activation of the free-base octakis-(phenylethynyl) compound lead to formal reduction of the porphyrin backbone via H-atom addition at opposing *meso*-positions. Generation of a common product suggests that both thermal and photochemical pathways to Bergman cyclization in solution contain significant activation barriers to formation of the 1,4-phenyl diradical intermediate, and under these solution conditions, alternate reaction channels are more thermodynamically favorable.

Introduction

Eneidyne are intriguing chemical structures that can undergo rearrangement to form a 1,4-phenyl diradical intermediate upon thermal^{1–12} or photochemical^{13–22} activa-

tion, ultimately leading to H-atom abstraction from DNA and cell death.²³ The geometric factors, i.e., distance between the alkyne termini,^{7,10,24} and strain in the ground and

* Author to whom correspondence should be addressed. E-mail: zaleski@indiana.edu.

- (1) Lee, M. D.; Dunne, T. S.; Chang, C. C.; Ellestad, G. A.; Siegel, M. M.; Morton, G. O.; McGahren, W. J.; Borders, D. B. *J. Am. Chem. Soc.* **1987**, *109*, 3466–3468.
- (2) Lee, M. D.; Dunne, T. S.; Siegel, M. M.; Chang, C. C.; Morton, G. O.; Borders, D. B. *J. Am. Chem. Soc.* **1987**, *109*, 3464–3466.
- (3) Lee, M. D.; Dunne, T. S.; Chang, C. C.; Ellestad, G. A.; Siegel, M. M.; Morton, G. O.; McGahren, W. J.; Borders, D. B. *J. Am. Chem. Soc.* **1992**, *114*, 985–997.

- (4) Golik, J.; Clardy, J.; Dubay, G.; Groenewold, G.; Kawaguchi, H.; Konishi, M.; Krishnan, B.; Ohkuma, H.; Saitoh, K.-i.; Doyle, T. W. *J. Am. Chem. Soc.* **1987**, *109*, 3461–3462.
- (5) Golik, J.; Dubay, G.; Groenewold, G.; Kawaguchi, H.; Konishi, M.; Krishnan, B.; Ohkuma, H.; Saitoh, K.; Doyle, T. W. *J. Am. Chem. Soc.* **1987**, *109*, 3462–3464.
- (6) Konishi, M.; Ohkuma, H.; Tsuno, T.; Oki, T.; VanDuyne, G. D.; Clardy, J. *J. Am. Chem. Soc.* **1990**, *112*, 3715–3716.
- (7) Nicolaou, K. C.; Ogawa, Y.; Zuccarello, G.; Schweiger, E. J.; Kumazawa, T. *J. Am. Chem. Soc.* **1988**, *110*, 4866–4868.
- (8) Nicolaou, K. C.; Smith, A. L.; Wendeborn, S. V.; Hwang, C.-K. *J. Am. Chem. Soc.* **1991**, *113*, 3106–3114.

transition states,^{25–28} as well as electronic contribution from electron-donating or -withdrawing substitution at the ene^{29–31} or yne³² positions of the 1,5-diyn-3-ene unit, can lead to dramatic influences on thermal cyclization temperatures. More recently, metal ions have also begun to play a key role in influencing the geometric contributions to enediyne cyclization by affecting the alkyne termini separation through chelation^{33–44} or π -complexation.^{45,46}

Although a considerable amount is known about the geometric and electronic factors that drive Bergman cyclization thermally, by comparison little is known about the origin of photo-Bergman cyclization,⁴⁷ and published examples are generally restricted to high-energy UV excitation.^{15–22} This is due to the ability of high-energy π – π^* transition of the enediyne unit to create a transient electronic structure that produces a subtle geometric distortion in the excited state, leading to the formation of the 1,4-phenyl diradical intermediate for some structures. In this sense, the photocyclization mechanism can be considered as an excited-state thermal reaction with a specific activation barrier to the formation of chemical intermediates or products.⁴⁷

In light of the tissue transparency advantages of red and near-infrared wavelengths, strongly absorbing chromophores at low energies are highly desirable for in vivo biological applications such as photodynamic therapy (PDT).^{48–51} Due to this requirement, the use of simple enediyne structures in these applications has not been widespread because of the contradictory relationship between practical depth penetration requirements and the need for UV excitation to initiate Bergman cyclization.

The widespread use of porphyrins in PDT applications, coupled with our interest in designing long-wavelength-absorbing enediyne motifs, and the recent enediyne-generated picenoporphyrin by Smith et al.,⁵² naturally led us to consider the porphyrin skeleton as a chromophore. Recent interest in alkynylated porphyrins for biological and materials applications has made incorporation of alkynes into such macrocycles synthetically accessible.^{52–57} Porphyrins have a rich electronic structure typically exhibiting strong electronic transitions throughout the visible spectral region (400–700 nm) with significant absorptivities ($\epsilon > 10000 \text{ M}^{-1} \text{ cm}^{-1}$).⁵⁸ In addition, these compounds also adopt distinctive saddled, ruffled, waved, or domed geometric conformations as a function of the central cation.^{59–61} The differing geometric

- (9) Nicolaou, K. C.; Dai, W.-M.; Tsay, S.-C.; Estevez, V. A.; Wrasidlo, W. *Science* **1992**, *256*, 1172–1178.
- (10) Nicolaou, K. C.; Zuccarello, G.; Riemer, C.; Estevez, V. A.; Dai, W.-M. *J. Am. Chem. Soc.* **1992**, *114*, 7360–7371.
- (11) Nicolaou, K. C.; Smith, A. L.; Yue, E. W. *Proc. Natl. Acad. Sci. U.S.A.* **1993**, *90*, 5881–5888.
- (12) Nicolaou, K. C.; Pitsinos, E. N.; Theodorakis, E. A.; Saimoto, H.; Wrasidlo, W. *Chem. Biol.* **1994**, *1*, 57–66.
- (13) Uesawa, Y.; Kuwahara, J.; Sugiura, Y. *Biochem. Biophys. Res. Commun.* **1989**, *164*, 903–911.
- (14) Sugiura, Y.; Shiraki, T.; Konishi, M.; Oki, T. *Proc. Natl. Acad. Sci. U.S.A.* **1990**, *87*, 3831–3835.
- (15) Nicolaou, K. C.; Dai, W.-M.; Wendeborn, S. V.; Smith, A. L.; Torisawa, Y.; Maligres, P.; Hwang, C.-K. *Angew. Chem., Int. Ed. Engl.* **1991**, *30*, 1032–1036.
- (16) Wender, P. A.; Zercher, C. K.; Beckham, S.; Haubold, E.-M. *J. Org. Chem.* **1993**, *58*, 5867–5869.
- (17) Funk, R. L.; Young, E. R. R.; Williams, R. M.; Flanagan, M. F.; Cecil, T. L. *J. Am. Chem. Soc.* **1996**, *118*, 3291–3292.
- (18) Evenzahav, A.; Turro, N. J. *J. Am. Chem. Soc.* **1998**, *120*, 1835–1841.
- (19) Kaneko, T.; Takahashi, M.; Hiram, M. *Angew. Chem., Int. Ed.* **1999**, *38*, 1267–1268.
- (20) Choy, N.; Blanko, B.; Wen, J.; Krishan, A.; Russell, K. C. *Org. Lett.* **2000**, *2*, 3761–3764.
- (21) Jones, G. B.; Wright, J. M.; Plourde, G., II; Purohit, A. D.; Wyatt, J. K.; Hynd, G.; Fouad, F. *J. Am. Chem. Soc.* **2000**, *122*, 9872–9873.
- (22) Purohit, A.; Wyatt, J.; Hynd, G.; Wright, J.; El-Shafey, A.; Swamy, N.; Ray, R.; Jones, G. B. *Tetrahedron Lett.* **2001**, *42*, 8579–8582.
- (23) Smith, A. L.; Nicolaou, K. C. *J. Med. Chem.* **1996**, *39*, 2103–2117.
- (24) Nicolaou, K. C.; Dai, W.-M.; Hong, Y. P.; Tsay, S.-C.; Baldrige, K. K.; Siegel, J. S. *J. Am. Chem. Soc.* **1993**, *115*, 7944–7953.
- (25) Magnus, P.; Lewis, R. T.; Huffman, J. C. *J. Am. Chem. Soc.* **1988**, *110*, 6921–6923.
- (26) Magnus, P.; Fortt, S.; Pitterna, T.; Snyder, J. P. *J. Am. Chem. Soc.* **1990**, *112*, 4986–4987.
- (27) Snyder, J. P. *J. Am. Chem. Soc.* **1989**, *111*, 7630–7632.
- (28) Snyder, J. P. *J. Am. Chem. Soc.* **1990**, *112*, 5367–5369.
- (29) Schreiner, P. R. *J. Am. Chem. Soc.* **1998**, *120*, 4184–4190.
- (30) Jones, G. B.; Warner, P. M. *J. Am. Chem. Soc.* **2001**, *123*, 2134–2145.
- (31) Jones, G. B.; Wright, J. M.; Hynd, G.; Wyatt, J. K.; Warner, P. M.; Huber, R. S.; Li, A.; Kilgore, M. W.; Sticca, R. P.; Pollenz, R. S. *J. Org. Chem.* **2002**, *67*, 5727–5732.
- (32) Prall, M.; Wittkopp, A.; Fokin, A. A.; Schreiner, P. R. *J. Comput. Chem.* **2001**, *22*, 1605–1614.
- (33) Warner, B. P.; Millar, S. P.; Broene, R. D.; Buchwald, S. L. *Science* **1995**, *269*, 814–816.
- (34) König, B.; Pitsch, W.; Thondorf, I. *J. Org. Chem.* **1996**, *61*, 4258–4261.
- (35) Basak, A.; Shain, J. C. *Tetrahedron Lett.* **1998**, *39*, 3029–3030.
- (36) Basak, A.; Shain, J. C.; Khamrai, U. K.; Rudra, K. R.; Basak, A. J. *Chem. Soc., Perkin Trans. 1* **2000**, 1955–1964.
- (37) Coalter, N. L.; Concolino, T. E.; Streib, W. E.; Hughes, C. G.; Rheingold, A. L.; Zaleski, J. M. *J. Am. Chem. Soc.* **2000**, *122*, 3112–3117.
- (38) Benites, P. J.; Rawat, D. S.; Zaleski, J. M. *J. Am. Chem. Soc.* **2000**, *122*, 7208–7217.
- (39) Schmitt, E. W.; Huffman, J. C.; Zaleski, J. M. *Chem. Commun.* **2001**, 167–168.
- (40) Chandra, T.; Pink, M.; Zaleski, J. M. *Inorg. Chem.* **2001**, *40*, 5878–5885.
- (41) Rawat, D. S.; Benites, P. J.; Incarvito, C. D.; Rheingold, A. L.; Zaleski, J. M. *Inorg. Chem.* **2001**, *40*, 1846–1857.
- (42) Rawat, D. S.; Zaleski, J. M. *J. Am. Chem. Soc.* **2001**, *123*, 9675–9676.
- (43) König, B. *Eur. J. Org. Chem.* **2000**, 381–385.
- (44) Basak, A.; Rudra, K. R.; Bag, S. S.; Basak, A. J. *Chem. Soc., Perkin Trans. 1* **2002**, 1805–1809.

- (45) O'Connor, J. M.; Lee, L. I.; Gantzel, P.; Rheingold, A. L.; Lam, K.-C. *J. Am. Chem. Soc.* **2000**, *122*, 12057–12058.
- (46) O'Connor, J. M.; Friese, S. J.; Tichenor, M. *J. Am. Chem. Soc.* **2002**, *124*, 3506–3507.
- (47) Clark, A. E.; Davidson, E. R.; Zaleski, J. M. *J. Am. Chem. Soc.* **2001**, *123*, 2650–2657.
- (48) Boyle, R. W.; Dolphin, D. *Photochem. Photobiol.* **1996**, *64*, 469–485.
- (49) Mody, T. D.; Sessler, J. L., Eds. *Supramolecular Materials and Technologies*; Wiley: Chichester, U.K., 1999; Vol. 4.
- (50) Ali, H.; van Lier, J. E. *Chem. Rev.* **1999**, *99*, 2379–2450.
- (51) Bonnett, R.; Martinez, G. *Tetrahedron* **2001**, *57*, 9513–9547.
- (52) Aihara, H.; Jaquinod, L.; Nurco, D. J.; Smith, K. M. *Angew. Chem., Int. Ed.* **2001**, *40*, 3439–3441.
- (53) DiMaggio, S. G.; Lin, V. S.-Y.; Therien, M. J. *J. Org. Chem.* **1993**, *58*, 5983–5993.
- (54) DiMaggio, S. G.; Lin, V. S.-Y.; Therien, M. J. *J. Am. Chem. Soc.* **1993**, *115*, 2513–2515.
- (55) Faust, R.; Weber, C. *J. Org. Chem.* **1999**, *64*, 2571–2573.
- (56) Mitzel, F.; FitzGerald, S.; Beeby, A.; Faust, R. *Chem. Commun.* **2001**, 2596–2597.
- (57) Uyeda, H. T.; Zhao, Y.; Wostyn, K.; Asselberghs, I.; Clays, K.; Persoons, A.; Therien, M. J. *J. Am. Chem. Soc.* **2002**, *124*, 13806–13813.
- (58) Gouterman, M. In *The Porphyrins*; Dolphin, D., Ed.; Academic Press: New York, 1978; Vol. 3(A), pp 1–156.
- (59) Sparks, L. D.; Medforth, C. J.; Park, M.-S.; Chamberlain, J. R.; Ondrias, M. R.; Senge, M. O.; Smith, K. M.; Shelnutt, J. A. *J. Am. Chem. Soc.* **1993**, *115*, 581–592.
- (60) Shelnutt, J. A.; Song, X.-Z.; Ma, J.-G.; Jia, S.-L.; Jentzen, W.; Medforth, C. J. *Chem. Soc. Rev.* **1998**, *27*, 31–42.

conformations strongly influence the disposition of substituents at the porphyrin periphery and, in turn, can be affected by the steric bulk of the R groups.^{62–64} Remarkably, even with the extensive study of porphyrin structures, controversy still exists over how the electronic structure of the porphyrin skeleton is influenced by these geometric distortions,^{65–68} and whether the R groups play an active or passive role in governing geometric and electronic structure.^{65,69}

The intriguing geometric and electronic characteristics of porphyrin macrocycles, and the potential for using these structural properties to influence the reactivities of enediynes, have led to several fundamental questions regarding the development and potential application of porphyrinic enediyne structures. Can more than one enediyne unit be incorporated into the porphyrin backbone? What are the geometric structures of porphyrinic enediyne compounds, and how do the number and nature of the substituents affect the structures? Conversely, what is the influence of the porphyrin structure on the thermal reactivities of the enediyne unit? Additionally, how are the electronic structures of these compounds affected by conjugated periphery substitution? Are these geometric and electronic characteristics maintained in solution? Finally, does conjugation of the enediyne unit into the large chromophore permit enediyne photocyclization, or does it lead to delocalization of the reactive excited state and alternate reactivity?

To this end, we have prepared a series of porphyrinic enediyne structures with five, six, and eight alkyne substituents, and several have been crystallographically characterized. The X-ray structures indicate that the identity of the central cation plays a strong role in determining the degree of ground-state geometric distortion in the resulting compounds. However, more subtly, the specific nature of the deviations from planarity is governed by the number of substituents at the porphyrin periphery. These structural differences influence the observed Bergman cyclization temperatures of the compounds, which are shown to loosely correlate with the degree of planarity of the macrocycle. In addition, electronic and resonance Raman spectra show systematic conjugation of the alkyne units into the porphyrin π – π^* transitions, indicating participation by the enediyne unit in the overall electronic structure. Careful examination of spectral shifts as a function of structure reveal systematic

trends that reflect the degree of planarity of the macrocycle. Finally, solution thermal and photochemical reactivity of the octasubstituted free-base derivative lead to the same 5,15-dihydroporphyrin product, indicating that the thermal and photochemical reaction pathways are connected to a common product. These results reveal key criteria required for the design of second-generation porphyrinic enediyne structures with specific reactivities.

Experimental Section

Materials. All chemicals and solvents used were of the highest purity available from Aldrich and Fluka. Reactions were carried out under nitrogen using Schlenk techniques, and all air-sensitive solids were handled in an inert-atmosphere drybox. Benzene, methylene chloride, and tetrahydrofuran were dried and degassed according to literature methods.⁷⁰ The free-base and metalated porphyrinic enediynes were purified by flash chromatography using silica gel (200–440 mesh) or neutral alumina.

Physical Measurements. ¹H NMR and ¹³C NMR were recorded on a VXR 400 NMR spectrometer using the residual proton resonance of the solvent as an internal reference. The multiplicities of the ¹³C NMR signals were determined by the DEPT technique. Electronic absorption spectra were collected on a Perkin-Elmer Lambda 19 UV/vis/near-IR spectrometer at ambient temperature. Infrared spectra (KBr) were recorded on a Nicolet 510P FT IR spectrometer. Elemental analyses on all samples were obtained from Robertson Microlit Laboratories, Inc. Mass data (FD, MALDI, and FAB) were obtained at the University of Illinois using a Micromass Quattro-I mass spectrometer. Cyclic voltammetry measurements were made using a BAS E2 Epsilon potentiostat/galvanostat running at a scan rate of 200 mV/s. The electrochemical cell consisted of a 0.5 M TBA(PF₆)/THF solution containing a Pt working electrode and a Ag/AgCl reference, with ferrocene (Fc) added as an internal standard. Oxidation potentials are irreversible and thus are reported as peak potentials. Reduction potentials derive from reversible waves at scan rates of 200 mV/s. Differential scanning calorimetry (DSC) traces were recorded on a V4.1 Dupont 910 differential scanning calorimeter coupled to a DuPont thermal analyst 2100 at a heating rate of 10 °C min^{–1}. Photolyses were performed using a 1000 W XeHg lamp (Oriel no. 66021) at $\lambda \geq 420$ nm using a series of long-pass cutoff filters ($\lambda \geq 295, 345, 395,$ and 420 nm). Resonance Raman spectra were collected using an Ar⁺ ion laser (Coherent model I-70) operating at 457.9, 488.0, or 501.7 nm (50 mW at the sample). The backscattered light was collected with a Nikkor 85 mm 1:1.4 lens focused through a depolarizer (CVI) onto the entrance slit of an f/4 subtractive double monochromator equipped with 600 grooves/mm gratings (500 nm blaze) and a 6 mm band-pass slit (7 nm/mm). The output from the double monochromator was focused onto the entrance slit of an Acton Spectrapro 500i spectrograph (f/6.5) operating with a 1800 grooves/mm (500 nm blaze) grating. The dispersed scattering was then recorded with a back-illuminated liquid N₂ cooled CCD (Princeton Instruments) with a 30 mm \times 14.4 mm active area (2500 \times 600 pixel array).

(2,3,7,8,12,13,17,18-Octabromo-5,10,15,20-tetraphenylporphyrinato)nickel(II) (1Ni).⁷¹ To a solution of 2,3,7,8,12,13,17,18-octabromo-5,10,15,20-tetraphenylporphyrin⁷¹ (0.420 g, 0.33 mmol) in chloroform was added Ni(CH₃COO)₂·4H₂O (0.084 g, 0.33 mmol)

- (61) Shelnutt, J. A. In *The Porphyrin Handbook*; Smith, K. M., Guillard, R., Eds.; Academic: New York, 2000; Vol. 7, pp 167–223.
- (62) Alden, R. G.; Crawford, B. A.; Doolen, R.; Ondrais, M. R.; Shelnutt, J. A. *J. Am. Chem. Soc.* **1989**, *111*, 2070–2072.
- (63) Medforth, C. J.; Senge, M. O.; Smith, K. M.; Sparks, L. D.; Shelnutt, J. A. *J. Am. Chem. Soc.* **1992**, *114*, 9859–9869.
- (64) Jentzen, W.; Simpson, M. C.; Hobbs, J. D.; Song, X.; Ema, T.; Nelson, N. Y.; Medforth, C. J.; Smith, K. M.; Veyrat, M.; Mazzanti, M.; Ramasseul, R.; Marchon, J.-C.; Takeuchi, T.; Goddard, W. A., III; Shelnutt, J. A. *J. Am. Chem. Soc.* **1995**, *117*, 11085–11097.
- (65) DiMaggio, S. G.; Wertsching, A. K.; Ross, C. R., II. *J. Am. Chem. Soc.* **1995**, *117*, 8279–8280.
- (66) Parusel, A. B. J.; Wondimagegn, T.; Ghosh, A. *J. Am. Chem. Soc.* **2000**, *122*, 6371–6374.
- (67) Wertsching, A. K.; Koch, A. S.; DiMaggio, S. G. *J. Am. Chem. Soc.* **2001**, *123*, 3932–3939.
- (68) Ryeng, H.; Ghosh, A. *J. Am. Chem. Soc.* **2002**, *124*, 8099–8103.
- (69) Wasbotten, I. H.; Wondimagegn, T.; Ghosh, A. *J. Am. Chem. Soc.* **2002**, *124*, 8104–8116.

- (70) Pangborn, A. B.; Giardello, M. A.; Grubbs, R. H.; Rosen, R. K.; Timmers, F. J. *Organometallics* **1996**, *15*, 1518–1520.
- (71) Bhyrappa, P.; Krishnan, V. *Inorg. Chem.* **1991**, *30*, 239–245.

in methanol, and the mixture was stirred for 24 h. After complete metalation, the solvent was removed under reduced pressure. The crude solid was suspended in methanol (50 mL) and allowed to stir for 1 h. The remaining solid was filtered, washed with methanol and subsequently with a mixture of methylene chloride/methanol (1:1), and dried under vacuum. Yield: 85%. Dark blue powder. MS (FD): m/z 1302 ($M^+ + 1$), 1224, 1145, 1065, 986, 908. Anal. Calcd for $C_{44}H_{20}Br_8N_4Ni \cdot 3H_2O$: C, 39.19; H, 1.94; N, 4.15. Found: C, 38.79; H, 1.76; N, 3.77. IR (KBr, cm^{-1}): 2967, 1598, 1574, 1443, 1323, 1128, 1069, 1042, 1025, 927, 752, 736, 615.

[5,10,15,20-Tetraphenyl-2,3,8,17,18-pentakis(phenylethynyl)porphinato]nickel(II) (NiP(PA)₅, 2Ni). To a crude (multiply brominated species) mixture of **1Ni** (0.5 g, 0.384 mmol) in dry, degassed THF (20 mL) was added $[(C_6H_5)_3P]_4Pd$ (0.2 g, 0.173 mmol) under nitrogen, and the mixture was stirred for 15 min at 30 °C. A solution of trimethyl(phenylethynyl)tin (0.92 g, 3.4 mmol) was prepared in degassed THF, and slowly added to the above mixture at 50 °C. The resulting solution was then heated at 75 °C for 6 h. Complete conversion of the starting material was confirmed by TLC (benzene/hexane, 1:1) and 1H NMR. After completion, the reaction mixture was cooled and the THF was removed under reduced pressure. The crude mixture was dissolved in methylene chloride (50 mL), and silica gel (20 g) was added to the flask. Following removal of the solvent under reduced pressure, the resulting powder was loaded onto a silica gel column. The column was eluted with a 5–30% benzene/hexane concentration gradient, which yielded a mixture of penta- and hexasubstituted porphyrins and pure octaalkynylporphyrin. The penta- and hexaalkynylporphyrins were then separated and purified via preparative thin-layer chromatography using a benzene/hexane (1:1) cosolvent mobile phase. Yield: 5% (pentaalkynylporphyrin, **2Ni**), 7% (hexaalkynylporphyrin, **3Ni**), and 40% (octaalkynylporphyrin, **4Ni**). Suitable crystals of **2Ni**–**4Ni** for X-ray diffraction were grown from a mixture of methanol and chloroform. The following are data for **2Ni**: R_f 0.7. Green solid. 1H NMR ($CDCl_3$): δ 7.27–7.31 (m, 25H, Ar), 7.59–7.67 (m, 12H, *meso*-Ar), 7.96–8.02 (m, 8H, *meso*-Ar), 8.59 (s, 2H, pyrrole), 8.87 (s, 1H, pyrrole). MS (FD): m/z 1170 (M^+), 1070, 970. Anal. Calcd for $C_{84}H_{48}N_4Ni \cdot H_2O$: C, 84.82; H, 4.24; N, 4.71. Found: C, 84.56; H, 4.52; N, 4.16. IR (KBr, cm^{-1}): 2922, 2187, 1596, 1558, 1539, 1506, 1489, 1456, 1341, 1260, 1101, 1013, 753, 688.

[5,10,15,20-Tetraphenyl-2,3,7,8,12,13-hexakis(phenylethynyl)porphinato]nickel(II) (NiP(PA)₆, 3Ni). R_f 0.6. Dark green solid. 1H NMR ($CDCl_3$): δ 7.26 (br s, 30H, Ar), 7.55–7.72 (m, 12H, *meso*-Ar), 8.05 (d, $J = 7.2$ Hz, 4H, *meso*-Ar), 8.16 (d, $J = 7.2$ Hz, 4H, *meso*-Ar), 8.45 (s, 2H, pyrrole). MS (FD): m/z 1271 ($M^+ + 1$), 970. Anal. Calcd for $C_{92}H_{52}N_4Ni \cdot H_2O$: C, 85.69; H, 4.22; N, 4.34. Found: C, 85.97; H, 4.52; N, 4.16. IR (KBr, cm^{-1}): 3051, 2920, 2850, 2189, 1595, 1518, 1440, 1397, 1338, 1255, 1222, 1103, 1003, 751, 687.

[5,10,15,20-Tetraphenyl-2,3,7,8,12,13,17,18-octakis(phenylethynyl)porphinato]nickel(II) (NiP(PA)₈, 4Ni). This compound was also prepared from pure **1Ni** as follows: To a suspension of **1Ni** (0.40 g, 0.30 mmol) in THF (20 mL) was added $[(C_6H_5)_3P]_4Pd$ (0.20 g, 0.17 mmol) under nitrogen, and the mixture was stirred for 15 min. A solution of trimethyl(phenylethynyl)tin (0.97 g, 3.6 mmol) in THF (30 mL) was added dropwise over 30 min at 50 °C. The temperature was raised to 70 °C and the solution refluxed for 8 h. Completion of the reaction was determined by TLC and 1H NMR. The solvent was then removed under reduced pressure, and the residue was extracted with methylene chloride (200 mL). The organic layer was dried over anhydrous sodium sulfate and evaporated under reduced pressure. The residue was then passed

through a silica gel column and eluted with benzene/hexane (1:1) to give the desired product in 65% yield. The crude solid was recrystallized in chloroform/benzene (1:1) to give needle-shaped green crystals. X-ray-quality crystals were grown from chloroform/methanol (1:1). R_f 0.5. 1H NMR ($CDCl_3$): δ 7.23 (br s, 40H, Ar), 7.58 (t, $J = 7.2$ Hz, 4H, *meso*-Ar), 7.69 (t, $J = 7.6$ Hz, 8H, *meso*-Ar), 8.19 (d, $J = 7.2$ Hz, 8H, *meso*-Ar). ^{13}C NMR ($CDCl_3$): δ 84.19 (Cquat), 105.43 (Cquat), 119.70 (Cquat), 123.53 (Cquat), 127.70 (CH), 127.84 (CH), 128.11 (CH), 129.92 (CH), 131.92 (CH), 132.07 (Cquat), 135.35 (CH), 137.80 (Cquat), 144.34 (Cquat). MS (FD): m/z 1471 ($M^+ + 1$), 1370, 1269, 1094, 925. Anal. Calcd for $C_{108}H_{60}N_4Ni \cdot H_2O$: C, 87.09; H, 4.16; N, 3.76. Found: C, 87.01; H, 4.09; N, 3.74. IR (KBr, cm^{-1}): 3051, 2192, 1652, 1596, 1530, 1495, 1441, 1259, 1105, 1003, 752, 688, 667.

[5,10,15,20-Tetraphenyl-2,3,7,8,12,13,17,18-octakis(phenylethynyl)porphyrin] (H₂P(PA)₈, 4H₂). To a suspension of pure 2,3,7,8,12,13,17,18-octabromo-5,10,15,20-tetraphenylporphyrin⁷¹ (**1H₂**) (1.0 g, 0.80 mmol) and $[(C_6H_5)_3P]_4Pd$ (0.2 g, 0.17 mmol) in THF (10 mL) was added trimethyl(phenylethynyl)tin (2.0 g, 7.5 mmol), and the reaction mixture was refluxed for 5 h. The reaction mixture was cooled to room temperature, and the solvent was then removed under reduced pressure. The residue was passed through a silica gel column and eluted with methylene chloride/hexane (1:1) to give the desired product as a dark brown solid. Yield: 70%. R_f 0.3. 1H NMR ($CDCl_3$): δ 7.21–7.30 (m, 40H, Ar), 7.65 (t, $J = 7.6$ Hz, 4H, *meso*-Ar), 7.77 (t, $J = 7.6$ Hz, 8H, *meso*-Ar), 8.42 (d, $J = 6.8$ Hz, 8H, *meso*-Ar), 9.62 (br s, 2H, 2NH). ^{13}C NMR ($CDCl_3$): δ 84.70 (Cquat), 104.09 (Cquat), 119.99 (Cquat), 123.52 (Cquat), 127.85 (CH), 128.17 (CH), 130.12 (CH), 131.26 (CH), 132.06 (CH), 135.01 (Cquat), 136.52 (CH), 139.14 (Cquat), 154.00 (Cquat). MS (FAB): m/z 1416 ($M^+ + 1$). Anal. Calcd for $C_{108}H_{62}N_4 \cdot H_2O$: C, 90.47; H, 4.50; N, 3.90. Found: C, 90.18; H, 4.22; N, 3.46. IR (KBr, cm^{-1}): 3320, 3051, 2188, 1652, 1596, 1504, 1478, 1441, 1404, 1343, 1275, 1089, 1069, 1000, 753, 688, 678.

[5,10,15,20-Tetraphenyl-2,3,7,8,12,13,17,18-octakis(phenylethynyl)porphinato]zinc(II) (ZnP(PA)₈, 4Zn). To a solution of **4H₂** (0.260 g, 0.183 mmol) in chloroform (20 mL) was added a solution of $Zn(CH_3COO)_2 \cdot 2H_2O$ (0.040 g, 0.182 mmol) in methanol (5 mL), and the resulting mixture was stirred for 4 h at room temperature. After the completion of the reaction, the solvent was removed under reduced pressure and the crude residue was suspended in methanol/chloroform (3:1) at 5 °C for 2 h. The solid was filtered, washed with hexane (2 × 20 mL), and then passed through a plug column using methylene chloride as the eluent. Suitable crystals for X-ray diffraction were grown from slow evaporation of chloroform in methanol. Yield: 92%. Metallic green crystalline solid. 1H NMR ($CDCl_3$): δ 7.19–7.26 (m, 25H, Ar), 7.32–7.34 (m, 15H, Ar), 7.60 (t, $J = 8$ Hz, 4H, *meso*-Ar), 7.72 (t, $J = 8$ Hz, 8H, *meso*-Ar), 8.33 (d, $J = 7.2$ Hz, 8H, *meso*-Ar). ^{13}C NMR ($CDCl_3$): δ 85.50 (Cquat), 104.59 (Cquat), 120.70 (Cquat), 123.91 (Cquat), 127.47 (CH), 127.77 (CH), 127.93 (CH), 130.18 (CH), 132.10 (CH), 132.77 (Cquat), 135.86 (CH), 140.27 (Cquat), 148.00 (Cquat). MS (FAB): m/z 1478 ($M^+ + 1$), 1347, 1290, 1240, 1175. Anal. Calcd for $C_{108}H_{60}N_4Zn \cdot 2H_2O$: C, 85.57; H, 4.25; N, 3.69. Found: C, 85.82; H, 4.50; N, 3.80. IR (KBr, cm^{-1}): 3051, 2189, 1594, 1569, 1511, 1492, 1402, 1384, 1323, 1258, 1174, 1104, 1068, 1001, 828, 752, 686.

[5,10,15,20-Tetraphenyl-2,3,7,8,12,13,17,18-octakis(phenylethynyl)porphinato]magnesium(II) (MgP(PA)₈, 4Mg). A solution of **4H₂** (100 mg, 0.070 mmol) in methylene chloride (15 mL) was charged with MgI_2 (140 mg, 0.50 mmol) and diisopropylethylamine (0.20 g, 1.5 mmol), and the mixture was stirred at 40 °C for 4 h. The reaction was monitored by TLC. After completion, ethanol

(1.0 mL) was added to the deeply colored mixture. The solution was then diluted with methylene chloride (50 mL) and washed with saturated sodium bicarbonate solution (2×50 mL). The organic layer was washed with water (50 mL), dried over sodium sulfate, and concentrated under reduced pressure. The residue was purified on silica gel with methylene chloride/hexane (1:1) to give **4Mg** in 80% yield as a metallic green crystalline solid. X-ray-quality crystals were obtained by slow evaporation of a 1:1 chloroform/methanol solution. ^1H NMR (CDCl_3): δ 7.20–7.26 (m, 25H, Ar), 7.32–7.35 (m, 15H, Ar), 7.16 (t, $J = 7.6$ Hz, 4H, *meso*-Ar), 7.73 (t, $J = 7.6$ Hz, 8H, *meso*-Ar), 8.36 (d, $J = 7.2$ Hz, 8H, *meso*-Ar). ^{13}C NMR (CDCl_3): δ 85.76 (Cquat), 103.70 (Cquat), 121.75 (Cquat), 123.98 (Cquat), 127.41 (CH), 127.76 (CH), 127.81 (CH), 129.93 (CH), 132.06 (CH), 132.32 (Cquat), 136.31 (CH), 140.86 (Cquat), 148.44 (Cquat). MS (MALDI-TOF): m/z 1438 ($\text{M}^+ + 1$). Anal. Calcd for $\text{C}_{108}\text{H}_{60}\text{N}_4\text{Mg}\cdot 4\text{H}_2\text{O}$: C, 85.91; H, 4.54; N, 3.71. Found: C, 85.54; H, 4.72; N, 3.71. IR (KBr, cm^{-1}): 3051, 2963, 2186, 1635, 1594, 1491, 1440, 1384, 1319, 1256, 1175, 1102, 1086, 1000, 975, 898, 825, 752, 688.

[5,10,15,20-Tetraphenyl-2,3,7,8,12,13,17,18-octakis(phenylethynyl)porphinato]copper(II) (Cu(PA)₈, 4Cu). To a solution of **4H₂** (0.060 g, 0.042 mmol) in chloroform was added $\text{Cu}(\text{CH}_3\text{COO})_2\cdot\text{H}_2\text{O}$ (0.010 g, 0.050 mmol) in methanol (5 mL), and the mixture was stirred until the starting material was completely converted to metalated product (3 h). The solvent was then removed under vacuum, and the residue was dissolved in methylene chloride and washed with water. The organic layer was dried over anhydrous sodium sulfate and concentrated in vacuo. The residue was then stirred in methanol at room temperature for 2 h. The solid was filtered, washed with methanol and hexane (2×20 mL), and then passed through a plug column using methanol/methylene chloride (1:9) as the eluent. Suitable crystals for X-ray diffraction were obtained by slow evaporation of chloroform in methanol. Black crystalline solid. R_f 0.4. MS (FD): m/z 1476 ($\text{M}^+ + 1$), 1378, 1277, 1179. Anal. Calcd for $\text{C}_{108}\text{H}_{60}\text{N}_4\text{Cu}\cdot\text{H}_2\text{O}$: C, 86.78; H, 4.18; N, 3.75. Found: C, 86.92; H, 4.22; N, 3.85. IR (KBr, cm^{-1}): 2963, 2187, 1652, 1594, 1440, 1260, 1102, 1021, 1001, 800, 749, 686.

[5,10,15,20-Tetraphenyl-2,3,7,8,12,13,17,18-octakis(trimethylsilylanylethynyl)porphyrin] (H₂P(TMSA)₈, 5H₂). Compound **5H₂** was prepared in a manner similar to that of **4H₂**. Freshly prepared trimethyl(trimethylsilylethynyl)tin was used in the $[(\text{C}_6\text{H}_5)_3\text{P}]_4\text{Pd}$ -catalyzed cross-coupling reaction. After workup, the crude product was purified on silica gel using a 1:1 mixture of hexane/methylene chloride as the eluent. Yield: 60%. Green crystalline solid. ^1H NMR (CDCl_3): δ 0.12 (s, 72H, 8SiCH₃), 7.68 (t, $J = 7.6$ Hz, 8H, *meso*-Ar), 7.80 (t, $J = 7.6$ Hz, 4H, *meso*-Ar), 8.18 (d, $J = 6.8$ Hz, 8H, *meso*-Ar). ^{13}C NMR (CDCl_3): δ 0.47 (CH₃), 97.46 (Cquat), 108.77 (Cquat), 120.40 (Cquat), 127.60 (CH), 129.62 (CH), 132.83 (Cquat), 137.03 (CH), 139.57 (Cquat), 153.89 (Cquat). MS (FD): m/z 1383 ($\text{M}^+ + 1$). Anal. Calcd for $\text{C}_{84}\text{H}_{94}\text{N}_4\text{Si}_8\cdot\text{H}_2\text{O}$: C, 71.97; H, 6.90; N, 3.75. Found: C, 71.78; H, 6.91; N, 3.75. IR (KBr, cm^{-1}): 3319, 2956, 2897, 2137, 1527, 1476, 1445, 1389, 1246, 1116, 1030, 1001, 926, 861, 842, 757, 732, 715.

[5,10,15,20-Tetraphenyl-2,3,7,8,12,13,17,18-octakis(trimethylsilylanylethynyl)porphinato]nickel(II) (NiP(TMSA)₈, 5Ni). To a solution of **5H₂** (0.230 g, 0.166 mmol) in chloroform (20 mL) was added a solution of $\text{Ni}(\text{CH}_3\text{COO})_2\cdot 4\text{H}_2\text{O}$ (0.041 g, 0.164 mmol) in methanol (5 mL), and the mixture was stirred at room temperature for 4 h. The solvent was removed under reduced pressure, and the crude product was purified on a silica gel column using methylene chloride/hexane (1:1). R_f 0.8. Yield: 83%. Green solid. ^1H NMR (CDCl_3): δ 0.089 (s, 72H, SiCH₃), 7.60 (t, $J = 7.6$ Hz, 8H, *meso*-

Ar), 7.73 (t, $J = 7.2$ Hz, 4H, *meso*-Ar), 7.95 (d, $J = 7.2$ Hz, 8H, *meso*-Ar). ^{13}C NMR (CDCl_3): δ 0.38 (CH₃), 96.95 (Cquat), 110.71 (Cquat), 120.07 (Cquat), 127.51 (CH), 129.52 (CH), 132.26 (Cquat), 135.54 (CH), 138.33 (Cquat), 145.46 (Cquat). MS (FD): m/z 1440 ($\text{M}^+ + 1$). Anal. Calcd for $\text{C}_{84}\text{H}_{92}\text{N}_4\text{Si}_8\text{Ni}\cdot 2\text{H}_2\text{O}$: C, 68.36; H, 6.56; N, 3.79. Found: C, 68.4; H, 6.17; N, 3.86. IR (KBr, cm^{-1}): 2956, 2897, 2139, 1506, 1414, 1362, 1330, 1246, 1165, 1140, 1007, 927, 865, 845, 757, 716.

[5,10,15,20-Tetraphenyl-2,3,7,8,12,13,17,18-octakis(trimethylsilylanylethynyl)porphinato]zinc(II) (ZnP(TMSA)₈, 5Zn). The preparation of **5Zn** is analogous to that of **4Zn**. Yield: 89%. Dark green solid. ^1H NMR (CDCl_3): δ 0.12 (s, 72H, SiCH₃), 7.65 (t, $J = 7.6$ Hz, 8H, *meso*-Ar), 7.79 (t, $J = 7.6$ Hz, 4H, *meso*-Ar), 8.13 (d, $J = 6.8$ Hz, 8H, *meso*-Ar). ^{13}C NMR (CDCl_3): δ 0.66 (CH₃), 97.97 (Cquat), 109.24 (Cquat), 121.36 (Cquat), 127.54 (CH), 129.54 (CH), 132.14 (Cquat), 136.66 (CH), 140.50 (Cquat), 148.64 (Cquat). MS (FD): m/z 1447 ($\text{M}^+ + 1$). Anal. Calcd for $\text{C}_{84}\text{H}_{92}\text{N}_4\text{Si}_8\text{Zn}\cdot 2\text{H}_2\text{O}$: C, 68.08; H, 6.53; N, 3.78. Found: C, 68.35; H, 6.62; N, 3.59. IR (KBr, cm^{-1}): 3056, 2957, 2898, 2136, 1601, 1489, 144, 1322, 1246, 1336, 1002, 901, 864, 756, 692.

[5,10,15,20-Tetraphenyl-2,3,7,8,12,13,17,18-octakis(trimethylsilylanylethynyl)porphinato]copper(II) (CuP(TMSA)₈, 5Cu). To a solution of **5H₂** (0.060 g, 0.043 mmol) in chloroform (20 mL) was added $\text{Cu}(\text{CH}_3\text{COO})_2\cdot\text{H}_2\text{O}$ (0.010 g, 0.050 mmol) in methanol (5 mL), and the reaction mixture was stirred for 2 h at room temperature. After the evaporation of the solvent, the crude product was washed several times with methanol (5×20 mL) and then dried under reduced pressure to afford **5Cu**. Yield: 85%. Dark green solid. MS (FD): m/z 1445 ($\text{M}^+ + 1$), 1351. Anal. Calcd for $\text{C}_{84}\text{H}_{92}\text{N}_4\text{Si}_8\text{Cu}\cdot\text{H}_2\text{O}$: C, 68.97; H, 6.48; N, 3.83. Found: C, 69.29; H, 6.58; N, 3.65. IR (KBr, cm^{-1}): 2956, 2897, 2139, 1615, 1500, 1496, 1444, 1354, 1325, 1246, 1168, 1138, 1003, 864, 845, 757, 738, 716, 694.

Photolysis of H₂P(PA)₈. Free-base **4H₂** (5 mg, 0.0035 mmol) was placed in a Schlenk flask and dried under vacuum. Degassed benzene-*d*₆ (0.6 mL) and excess (>100 -fold) 1,4-cyclohexadiene (CHD) were then added, and the solution was transferred to a J-Young NMR tube. The sealed tube was placed in a temperature-controlled (13 °C) bath and photolyzed with $\lambda \geq 420$ nm light for 6 h. Upon photolysis, the solution turned from green-brown to dark red. After completion of the reaction, the solvent was removed and the product was purified via preparative TLC using methylene chloride/hexane (1:1). The reaction was repeated on a ~ 50 mg scale in a Schlenk flask (18 h) using the same ratio of solvent to CHD and **4H₂** to CHD under parallel conditions. X-ray-quality crystals of $\text{H}_2\text{P(PA)}_8$ **6H₂** were obtained by slow evaporation of a 1:1 chloroform/methanol solution. Yield of octasubstituted 5,15-dihydroporphyrin product **6H₂**: 70%. R_f 0.5. ^1H NMR (CDCl_3): δ 6.45 (s, 2H, *meso*-CHR), 7.13–7.17 (m, 18H, Ar), 7.19–7.23 (m, 14H, Ar), 7.24–7.25 (m, 3H, Ar), 7.35–7.37 (m, 5H, Ar), 7.43–7.45 (m, 8H, *meso*-Ar), 7.48–7.53 (m, 4H, *meso*-Ar), 7.58–7.62 (m, 4H, *meso*-Ar), 7.65–7.67 (m, 4H, *meso*-Ar). ^{13}C NMR (CDCl_3): δ 82.23 (Cquat), 83.69 (Cquat), 98.38 (Cquat), 102.53 (Cquat), 119.89 (Cquat), 123.37 (Cquat), 126.33 (Cquat), 127.30 (Cquat), 127.82 (CH), 128.07 (Cquat), 128.17 (CH), 128.29 (CH), 129.19 (CH), 130.15 (CH), 130.76 (CH), 130.96 (CH), 131.52 (CH), 131.99 (CH), 134.59 (Cquat), 139.37 (Cquat), 139.57 (Cquat), 140.31 (Cquat), 157.16 (Cquat). MS (MALDI-TOF): m/z 1417 ($\text{M}^+ + 1$) 1308, 825, 809, 545, 523. Anal. Calcd for $\text{C}_{108}\text{H}_{64}\text{N}_4\cdot 2\text{H}_2\text{O}$: C, 89.22; H, 4.71; N, 3.85. Found: C, 89.27; H, 4.23; N, 3.77. IR (KBr, cm^{-1}): 2960, 2187, 1733, 1700, 1652, 1596, 1521, 1464, 1384, 1250, 1208, 1139, 1068, 998, 952, 752, 687.

Thermolysis of $\text{H}_2\text{P}(\text{PA})_8$. Under anaerobic conditions, a Schlenk flask was charged with $\mathbf{4H}_2$ (30 mg, 0.021 mmol) and 1,4-cyclohexadiene (1.2 g, 15 mmol) in 1,2,4-trichlorobenzene (20 mL), and the mixture degassed by three freeze–pump–thaw cycles. The mixture was transferred into a pressure vessel under nitrogen and heated at 250 °C in sand for 48 h. The reaction vessel was cooled and the reaction mixture passed through a silica gel column using hexane as the eluent for 1,2,4-trichlorobenzene. The product was then removed from the column with methylene chloride and repurified on silica gel using methylene chloride/hexane (1:1) as the eluent. Yield of octasubstituted 5,15-dihydroporphyrin product $\mathbf{6H}_2$: 67%. Using 2-propanol as a hydrogen donor gives a 73% yield of $\mathbf{6H}_2$. The spectroscopic data were identical to those of the photochemically prepared product $\mathbf{6H}_2$.

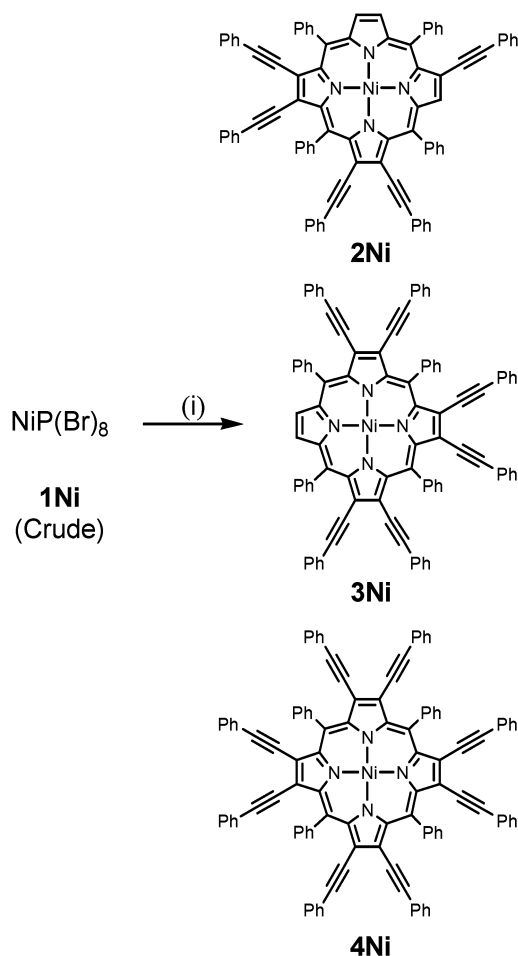
Photolysis and Thermolysis of 5,10,15,20-Tetraphenylporphyrin (H_2TPP). H_2TPP was photolyzed and thermolyzed (96 h) in the same manner as free-base $\mathbf{4H}_2$. Standard NMR and chromatographic analyses of the solutions revealed only the presence of unreacted H_2TPP starting material with no *meso*-reduced product formation.

X-ray Structure Determinations. X-ray-quality crystals of $\mathbf{2Ni}$ – $\mathbf{4Ni}$, $\mathbf{4H}_2$, $\mathbf{4Zn}$, $\mathbf{4Cu}$, and $\mathbf{4Mg}$ were grown by slow evaporation from either a methanol/dichloromethane or methanol/chloroform mixture (1:1). Crystals were mounted onto glass fiber mounting pins using a matrix of high-vacuum silicone grease. In cases where solvent loss was severe, the crystals were placed in a 0.05 mm monofilament loop with a solvent matrix. The crystals were immediately placed on a Bruker SMART6000 diffractometer and cooled using a locally designed nitrogen flow cooling system. The cooling system utilizes house nitrogen and a recooling Dewar with a silvered glass delivery tube. The sample temperature can be maintained from 110 K to room temperature as desired. The data were collected using a sealed, graphite-monochromatized Mo X-ray source. Data were collected using a combination of ω and ϕ scans, with frame widths of 0.30° and frame times selected on the basis of the scattering of the individual crystal. Data collection and initial indexing and cell refinement were handled using SMART software.⁷² Frame integration and final cell parameter calculation were carried out using SAINT software.⁷³ Where necessary, the data were corrected for absorption using the SADABS program.⁷⁴ Decay of reflection intensity was not observed. Structure solution and refinement, the production of graphics, and the preparation of publication materials were performed using SHELXTL and various local programs.⁷⁵

Results and Discussion

Syntheses. The starting materials $\mathbf{1Ni}$ and $\mathbf{1H}_2$ were prepared in good yields by standard literature procedures.⁷¹ Crude $\mathbf{1Ni}$ contains a mixture of penta-, hexa-, and octabrominated TPP due to incomplete bromination. Pure $\mathbf{1Ni}$ is obtained by extracting the hexa- and pentabromo derivatives by stirring the mixture in CH_2Cl_2 for 3 h. The octabromoporphyrin product, which is insoluble in CH_2Cl_2 , is then isolated by filtration. Tin alkynes⁷⁶ for subsequent Stille coupling^{77,78}

Scheme 1. Syntheses of $\text{NiP}(\text{PA})_5$, $\text{NiP}(\text{PA})_6$, and $\text{NiP}(\text{PA})_8$ ($\mathbf{2Ni}$ – $\mathbf{4Ni}$)^a



^a Reaction conditions: (i) trimethyl(phenylethynyl)tin, Pd(0), THF, reflux.

reactions were prepared from lithium salts of the corresponding alkynes at temperatures ranging from –78 to +20 °C. All metal-mediated coupling reactions^{52–54,79,80} were performed in refluxing THF under nitrogen.

Reaction of crude $\mathbf{1Ni}$ with trimethyl(phenylethynyl)tin over a Pd(0) catalyst in THF leads to the generation of a mixture of penta-, hexa-, and octaalkynylporphyrinic eneidyne $\mathbf{2Ni}$ – $\mathbf{4Ni}$ (Scheme 1). The products of the crude reaction were purified on silica gel using a 1:1 mixture of benzene/hexane as the eluent. Compound $\mathbf{4Ni}$ was isolated and recrystallized from a methanol/chloroform mixture (1:1). The structure was confirmed by ^1H NMR, ^{13}C NMR, and mass spectrometry, as well as X-ray crystallography (vide infra). In the ^1H NMR spectrum of $\mathbf{4Ni}$, a broad singlet appears at δ 7.23 for the eight phenyl rings of the phenylacetylene units. Two triplets and one doublet are observed at δ 7.58 and 7.69 and δ 8.19, respectively, for the protons of the *meso*-phenyl groups. The presence of the alkyne carbons is verified by resonances at δ 84.19 and 105.43 in the ^{13}C NMR. Compound $\mathbf{4Ni}$ was also prepared indepen-

(72) SMART, Version 4.210, Bruker Analytical X-ray Systems, 6300 Enterprise Lane, Madison, WI 53719, 1996.

(73) SAINT, Version 4.05, Bruker Analytical X-ray Systems, 6300 Enterprise Lane, Madison, WI 53719, 1996.

(74) Sheldrick, G. SADABS; University of Göttingen: Göttingen, Germany, 1996.

(75) SHELXTL, Version 5.1, Bruker Analytical X-ray Systems, 6300 Enterprise Lane, Madison, WI 53719, 1997.

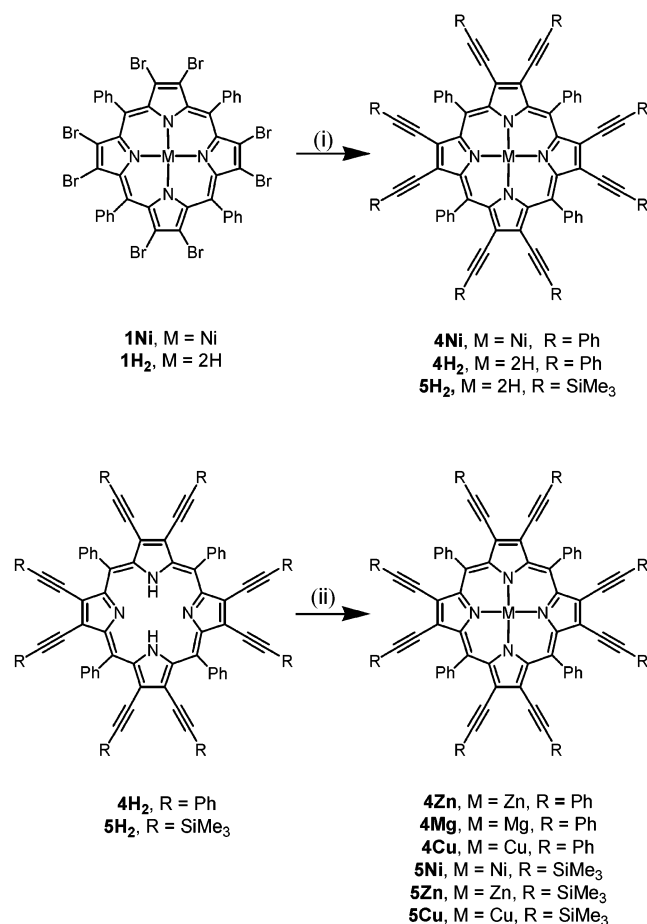
(76) Menz, G.; Wrackmeyer, B. *Z. Naturforsch., B* **1977**, 32B, 1400–1407.

(77) Stille, J. K. *Angew. Chem.* **1986**, 98, 504–519.

(78) Stille, J. K. *Angew. Chem., Int. Ed. Engl.* **1986**, 25, 508–524.

(79) Heck, R. F. *Acc. Chem. Res.* **1979**, 12, 146–151.

(80) Lin, V. S.-Y.; DiMaggio, S. G.; Therien, M. J. *Science* **1994**, 264, 1105–1111.

Scheme 2. Syntheses of Octaalkynylporphyrinic Enediyne Derivatives **4** and **5**^a

^a Reaction conditions: (i) trimethyl(phenylethynyl)tin/trimethyl(trimethylsilyl)ethynyltin, Pd(0), THF, reflux; (ii) M(OAc)₂·H₂O, MeOH, CHCl₃, rt/MgI₂, diisopropylethylamine, 40 °C, 4 h.

dently in 65% yield by reacting pure **1** with the same tin reagent under identical coupling conditions (Scheme 2).

The free-base porphyrinic enediynes **4H₂** and **5H₂** were similarly prepared in good yields (**4H₂**, 70%; **5H₂**, 60%) from 2,3,7,8,12,13,17,18-octabromo-5,10,15,20-tetraphenylporphyrin⁷¹ as described for **1Ni**, without using the metalloporphyrin template for the coupling reaction.⁸¹ Compound **5H₂** (H₂P-(TMSA)₈) was synthesized by reacting freshly prepared trimethyl(trimethylsilyl)ethynyltin⁷⁶ with **1H₂** under reflux in THF (Scheme 2). The structures of porphyrinic enediynes **4H₂** and **5H₂** were confirmed by ¹H NMR, ¹³C NMR, mass spectrometry, and X-ray crystallography (for **4H₂**). In the ¹H NMR of **5H₂**, a sharp singlet appears at δ 0.12 for the 72 protons of the trimethylsilyl groups. Two triplets and one doublet are also observed at δ 7.68 and 7.80 (triplet) and δ 8.18 (doublet) corresponding to resonances of the *meso*-phenyl rings. In the ¹³C NMR, the alkyne carbons are detected at δ 97.46 and 108.77.

The metalated octaalkynylporphyrinic enediynes **4Zn**, **4Mg**, **4Cu**, **5Zn**, **5Cu**, and **5Ni** were readily prepared from **4H₂** or **5H₂** using the corresponding metal acetate at room temperature (Scheme 2). The Mg(II) derivative **4Mg** was

Table 1. Crystallographic Data for **2Ni–4Ni**

	2Ni	3Ni	4Ni
empirical formula	C ₈₁ H ₅₁ Cl ₃ N ₄ Ni	C ₉₆ H ₆₀ Cl ₈ N ₄ Ni	C ₁₁₄ H ₆₆ Cl ₁₈ N ₄ Ni
fw	1245.37	1611.87	2188.52
cryst color	metallic black	black	black
cryst syst	monoclinic	triclinic	monoclinic
space group	<i>P</i> 2 ₁ / <i>c</i>	<i>P</i> $\bar{1}$	<i>C</i> 2/ <i>c</i>
<i>a</i> , Å	14.5157(7)	13.8989(17)	27.913(3)
<i>b</i> , Å	20.9515(11)	15.5193(21)	18.4655(16)
<i>c</i> , Å	19.6961(10)	19.0221(24)	17.9207(14)
α, deg	90	102.745(4)	90
β, deg	108.609(2)	96.614(4)	91.617(2)
γ, deg	90	104.401(3)	90
<i>V</i> , Å ³	5683.06	3812.9(14)	9233.2(14)
<i>Z</i>	4	2	4
ρ _{calcd} , g/cm ³	1.456	1.404	1.574
<i>T</i> , K	115	115	108
λ, Å	0.71073	0.071073	0.71073
refined on the basis of	<i>F</i>	<i>F</i>	<i>F</i> ²
GOF on <i>F</i> ²	1.498	1.864	0.905
final <i>R</i> indices ^a	<i>R</i> = 0.073	<i>R</i> = 0.065	<i>R</i> 1 = 0.076
[<i>I</i> > 2σ(<i>I</i>)]	<i>R</i> _w = 0.086	<i>R</i> _w = 0.057	w <i>R</i> 2 = 0.194
<i>R</i> indices ^a (all data)			<i>R</i> 1 = 0.162
			w <i>R</i> 2 = 0.230
largest diff peak and hole	1.064 and −0.83		0.973 and −0.547

^a *R*1 = Σ(|*F*_o| − |*F*_c|)/Σ|*F*_o|. w*R*2 = {Σ[w(*F*_o² − *F*_c²)²]/Σ[w(*F*_o²)²]}^{1/2}. *R* = Σ|*F*_o| − |*F*_c|/Σ|*F*_o|. *R*_w = {Σw[|*F*_o| − |*F*_c|]²/Σw|*F*_o|²}^{1/2}. *w* = 1/σ²(|*F*_o|).

prepared by Lindsey's method.⁸² Briefly, free-base **4H₂** was treated with MgI₂ in the presence of excess diisopropylethylamine at 40 °C, producing MgP(PA)₈ in 80% yield. Crystallization of **4Mg** from methanol/chloroform (1:1) leads to axial coordination of a solvent molecule (MeOH) in the X-ray structure (vide infra). In the ¹H NMR, the aromatic resonances of the phenylacetylene fragment appear at δ 7.20–7.26 as a multiplet for 25 protons. A second multiplet is also observed at δ 7.32–7.35 corresponding to 15 protons of the phenylacetylene unit. The *meso*-phenyl protons are observed at δ 7.16 and 7.73 as a triplet and δ 8.36 as a doublet. The identities of **4Zn**, **4Mg**, **5Ni**, and **5Zn** were confirmed by NMR, mass spectrometry, and elemental analysis, while the structures of **4Zn**, **4Mg**, and **4Cu** were characterized by X-ray diffraction. The paramagnetic compound **5Cu** was characterized by mass and elemental analysis.

X-ray Crystal Structures of Porphyrinic Enediynes. A summary of crystallographic data for the Ni-substituted porphyrinic enediyne structures **2Ni–4Ni** is given in Table 1, with the accompanying structures shown in Figure 1. Compounds **2Ni–4Ni** crystallize as black plates in monoclinic or triclinic space groups by slow evaporation from either 1:1 methanol/chloroform (for **2Ni** and **4Ni**) or methanol/methylene chloride (for **3Ni**). Crystals of the corresponding free-base, zinc(II), magnesium(II), and copper(II) octaalkynylporphyrin derivatives **4H₂**, **4Zn**, **4Mg**, and **4Cu** were grown by slow evaporation from chloroform (**4H₂**) or 1:1 chloroform/methanol mixtures (**4Zn** and **4Mg**). Crystals of **4Cu** were obtained by slow evaporation of a 1:1 chloroform/methanol cosolvent system. The resulting structures and crystallographic parameters are given in Figure 2 and Table 2, respectively. Like their Ni(II) counterparts, these com-

(81) Shea, K. M.; Jaquinod, L.; Smith, K. M. *J. Org. Chem.* **1998**, *63*, 7013–7021.

(82) O'Shea, D. F.; Miller, M. A.; Matsueda, H.; Lindsey, J. S. *Inorg. Chem.* **1996**, *35*, 7325–7338.

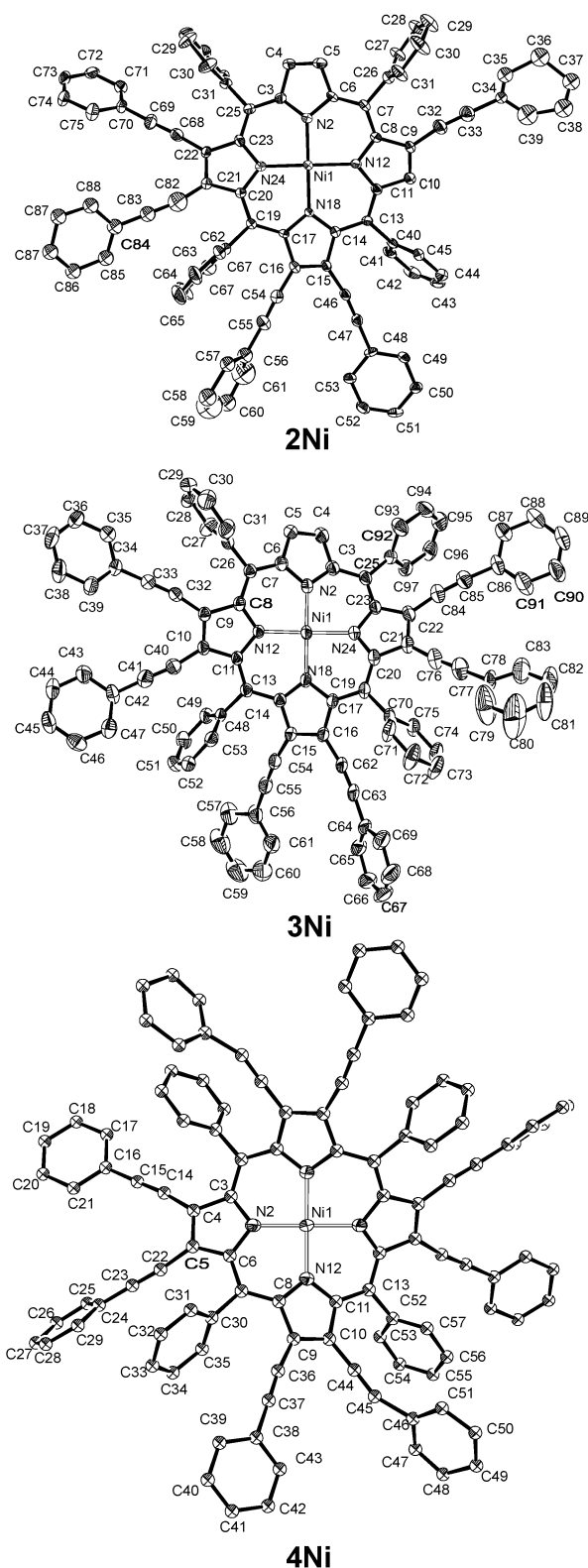


Figure 1. ORTEP representations of the X-ray crystal structures of **2Ni**–**4Ni**. Thermal ellipsoids are illustrated at 50% probability.

pounds crystallize as dark brown, black, or green materials in low-symmetry monoclinic or triclinic space groups (Table 2).

Each porphyrin possesses differing degrees of distortion depending upon the identity of the central cation and the number of phenylacetylene substituents at the β -pyrrole

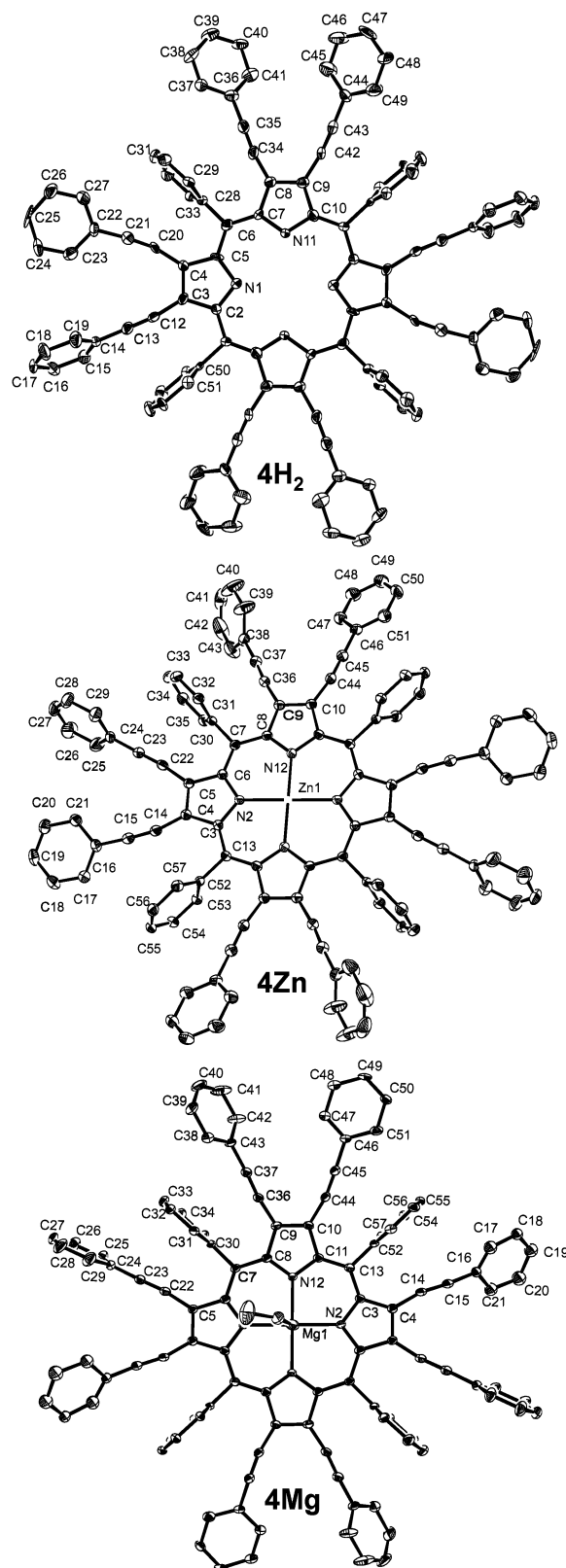


Figure 2. ORTEP representations of the X-ray crystal structures of **4H₂**, **4Zn**, **4Mg**, and **4Cu**. Thermal ellipsoids are illustrated at 50% probability.

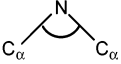
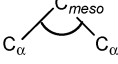
positions (Table 3). For the Ni(II) series **2Ni**–**4Ni**, the structures are all nonplanar, which is common for substituted nickel porphyrin derivatives.^{63,83–88} The pentaalkynyl derivative **2Ni** exhibits the classic ruffled conformation, while the hexasubstituted porphyrin **3Ni** and octaalkynyl compound

Table 2. Crystallographic Data for **4H₂**, **4Zn**, **4Mg**, and **4Cu**

	4H₂	4Zn	4Mg	4Cu
empirical formula	C ₁₀₈ H ₆₂ N ₄	C ₁₁₀ H ₆₂ Cl ₆ N ₄ Zn	C ₁₁₁ H ₆₅ N ₄ Cl ₆ Mg	C ₁₀₈ H ₆₀ CuN ₄
fw	1415.71	1717.84	1707.78	1477.24
cryst color	dark brown	metallic green	metallic green	black
cryst syst	triclinic	monoclinic	monoclinic	triclinic
space group	<i>P</i> $\bar{1}$	<i>P</i> 2 ₁ / <i>c</i>	<i>P</i> 2 ₁ / <i>c</i>	<i>P</i> $\bar{1}$
<i>a</i> , Å	12.1770(12)	15.2911(4)	15.3782(4)	11.8599(11)
<i>b</i> , Å	12.3303(13)	20.1741(5)	20.1494(5)	16.5714(15)
<i>c</i> , Å	14.3679(14)	13.5494(4)	13.8125(4)	20.8422(19)
α , deg	68.6847(27)	90.00(0)	90.00(0)	72.6033(23)
β , deg	70.9162(25)	99.2212(6)	98.713(1)	76.0427(23)
γ , deg	72.0008(28)	90	90	84.0341(26)
<i>V</i> , Å ³	1854.43	4125.8(3)	4230.57	3791.21
<i>Z</i>	1	2	2	2
ρ_{calcd} , g/cm ³	1.268	1.383	1.341	1.294
<i>T</i> , K	122	118	116	121
λ , Å	0.71073	0.71073	0.71073	0.71073
refined on the basis of	F	F	F	F
GOF	1.355	1.231	1.759	0.680
final <i>R</i> indices ^a [<i>I</i> > 2 σ (<i>I</i>)]	<i>R</i> = 0.076 <i>R</i> _w = 0.059	<i>R</i> = 0.046 <i>R</i> _w = 0.045	<i>R</i> = 0.065 <i>R</i> _w = 0.056	<i>R</i> = 0.040 <i>R</i> _w = 0.043
largest diff peak and hole	0.55 and −0.59	0.53 and −0.44	0.66 and −0.68	0.58 and −0.68

$$^a R = \sum(|F_o| - |F_c|)/\sum|F_o|. R_w = [\sum w(|F_o| - |F_c|)^2 / \sum w|F_o|^2]^{1/2}. w = 1/\sigma^2(|F_o|).$$

Table 3. Structural Parameters and Average Deviations from Planarity for **2–4**

compd	dev from plane ^a /Å	<i>C</i> _{meso} /Å	$\langle M-N \rangle$ /Å		
2Ni	0.285	0.595	1.932	106.13	121.60
3Ni	0.392	0.585	1.917	106.36	120.94
4Ni	0.451	0.617	1.918	106.60	120.67
4Cu	0.275	0.025	2.003	106.65	123.99
4H₂	0.068	0.091	109.16	126.05	
4Zn	0.030	0.034	2.057	107.50	125.69
4Mg	0.039	0.042	2.072	107.64	126.48

^a The deviation from the plane is defined as the mean deviation of the 24 core atoms of the macrocycle from the idealized planar structure.

4Ni exhibit complex distortions containing degrees of both ruffling and saddling.^{60,61} Features such as the average Ni–N bond length, the *C*_α–*C*_{meso}–*C*_α and *C*_α–N–*C*_α angles, and the observed mean deviation of the 24 core atoms of the macrocycle from planarity are diagnostic of these structural distortions (Table 3).

Within this series, the pentaalkynyl nickel porphyrin **2Ni** is the least distorted, having a mean deviation from the plane of 0.285 Å. The value of this parameter increases to 0.451 Å for the octaalkynyl derivative **4Ni**, revealing a systematic increase in distortion as a function of peripheral substitution. In these structures, the β -carbon of each pyrrole is tilted above and below the plane, which causes the phenylacetylene substituents to bend in opposite directions to their nearest neighbors. Additionally, the unsubstituted *C*_β–*C*_β (*C*4–*C*5) bond in **2Ni** is shorter (1.329(5) Å) than that of the substituted β -pyrrolic carbons (*C*21–*C*22 = 1.374(5) Å).

This trend is also observed in **3Ni** (*C*4–*C*5 = 1.362 Å vs *C*15–*C*16 = 1.385 Å) and **4Ni**, where the *C*_β–*C*_β distance is further increased to 1.388 Å. Lengthening of the *C*_β–*C*_β bond increases the ideal radial size of the porphyrin core,^{64,89} which is consistent with the increasing degree of distortion observed upon additional substitution. Within this Ni(II) series **2Ni**–**4Ni**, it is apparent that increasing peripheral substitution is responsible for the enhancement of the porphyrin ring distortion.

Unlike the highly distorted, partially ruffled/saddled structures of **2Ni**–**4Ni**, the crystal structure of **4H₂** shows a wave conformation (Figure 2, Table 3).⁸⁴ The structure is only slightly distorted with a mean deviation from planarity of 0.068 Å (Table 2), revealing that the distortions observed in **2Ni**–**4Ni** do not solely derive from steric strain between the peripheral groups. Interestingly, the *C*_β–*C*_β bond lengths of the four pyrrole units are almost identical (*C*3–*C*4 = 1.383(7) Å and *C*8–*C*9 = 1.381(7) Å), but the bond angles *C*2–N1–*C*5 (112.3(5)°) and *C*7–N11–*C*10 (105.0(4)°) show a large asymmetry.

The structure of the Zn(II) derivative **4Zn** is nearly planar, exhibiting only a very modest wave conformation with the *trans*-phenylacetylenes projecting in opposite directions from the mean plane of the porphyrin core (Figure 2, Table 3). The average Zn–N distance is 2.057 Å, consistent with the nearly planar nature of the 24-atom core. The structure of MgP(PA)₈, **4Mg**, is unique in that the Mg²⁺ ion is 5-coordinate with an axially bound methanol which is not detected in solution by NMR. The structure of **4Mg**, however, is very similar to that of **4Zn** in that the 24-atom core is nearly planar, and exhibits only a slight wave deformation, leading to only a small deviation from planarity (0.039 Å). For CuP(PA)₈, **4Cu**, a ruffle/saddle conformation is observed that is very similar to that of Cu(OETPP) reported by Sparks.⁵⁹ The distortion leads to an overall mean deviation from the plane of 0.275 Å, which is similar to that observed for **3Ni** and

(83) Senge, M. O.; Renner, M. W.; Kalisch, W. W.; Fajer, J. *J. Chem. Soc., Dalton Trans.* **2000**, 381–386.

(84) Nurco, D. J.; Medforth, C. J.; Forsyth, T. P.; Olmstead, M. M.; Smith, K. M. *J. Am. Chem. Soc.* **1996**, *118*, 10918–10919.

(85) Senge, M. O.; Bischoff, I. *Eur. J. Org. Chem.* **2001**, 1735–1751.

(86) Barkigia, K. M.; Renner, M. W.; Furenlid, L. R.; Medforth, C. J.; Smith, K. M.; Fajer, J. *J. Am. Chem. Soc.* **1993**, *115*, 3627–3635.

(87) Senge, M. O.; Kalisch, W. W. *Inorg. Chem.* **1997**, *36*, 6103–6116.

(88) Kalisch, W. W.; Senge, M. O. *Angew. Chem., Int. Ed.* **1998**, *37*, 1107–1109.

(89) Hoard, J. L. *Ann. N. Y. Acad. Sci.* **1973**, *206*, 18–31.

Table 4. Electronic Absorption Maxima (λ/nm ($\epsilon \times 10^{-4}/\text{M}^{-1} \text{cm}^{-1}$)) for Porphyrinic Eneidyne Collected at 25 °C in CH_2Cl_2

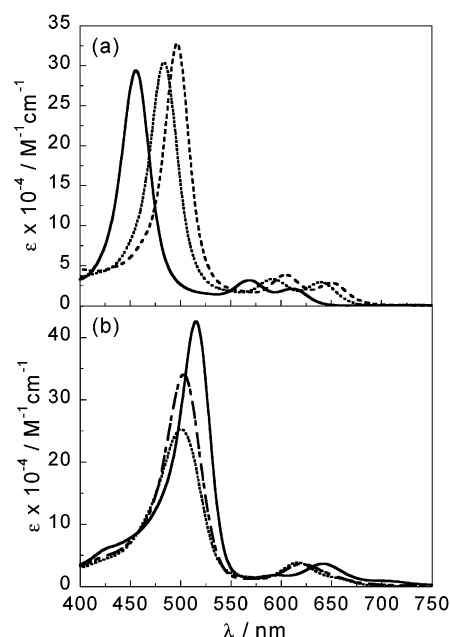
compd	B band	Q bands
2Ni	456 (29.34)	568 (3.14), 611 (2.08)
3Ni	484 (30.59)	592 (3.44), 639 (3.01)
4Ni	497 (32.80)	604 (3.84), 650 (2.85)
4Cu	500 (25.25)	616 (3.86), 655 (1.42)
4H₂	506 (30.36)	595 (3.70), 669 (1.10), 761 (0.32)
4Zn	503 (34.02)	620 (3.63)
4Mg	515 (42.58)	595 (1.82), 642 (3.66), 705 (0.09)
4Ni^a	499	608, 654
4Cu^a	505	615, 653
4H₂^a	508	582, 656, 750
4Zn^a	507	618
4Mg^a	510	585, 635
5Ni	487 (31.55)	597 (2.95), 639 (1.35)
5Cu	501 (23.66)	618 (3.21), 667 (0.50)
5H₂	502 (29.42)	596 (1.96), 651 (1.28), 764 (0.41)
5Zn	505 (25.68)	632 (1.61), 699 (0.63)
6H₂	520 (1.36)	600 (0.23)

^a Solid-state spectra collected in KBr at 25 °C.

4Ni, but with an overall distortion that is more comparable to that of **2Ni** in magnitude.

Comparison of the octaalkynyl analogues with various central cations (**4Ni**, **4H₂**, **4Zn**, **4Cu**, and **4Mg**) leads to an interesting trend in the degree of distortion of the compounds. Due to the static substitution pattern across the series, the effect must derive exclusively from the identity of the central metal ion. Using the mean deviation of the 24 core atoms of the porphyrin ring as the measure of distortion, the deviation increases in the order $\text{Zn} < \text{Mg} < \text{H}_2 < \text{Cu} < \text{Ni}$ (Table 3). Although this order is in slight contrast to that obtained by other common measures of distortion, including the M–N bond length, the $\text{C}_\alpha\text{--C}_{\text{meso}}\text{--C}_\alpha$ angle, and the $\text{C}_\alpha\text{--N--C}_\alpha$ angle, it is clear from the magnitude of the mean deviation that **4Mg** and **4Zn** are very similar (0.039 and 0.030 Å, respectively), and as a result, the degree of nonplanarity is best represented as $\text{Mg} \approx \text{Zn} < \text{H}_2 < \text{Cu} < \text{Ni}$.

Electronic Spectroscopy. The electronic absorption spectra of the octaalkynylporphyrins show dramatic red shifts in both the Soret and Q bands (Table 4). Generally, these derivatives have electronic spectra that are shifted by ~ 100 nm relative to their unsubstituted counterparts.⁹⁰ Interestingly, the β -phenylacetylene substitution has a larger effect on the optical spectra than benzannulation of the pyrroles, as the octaalkynyl derivatives have electronic spectra that are red-shifted by ~ 30 nm relative to that of tetraphenyltetraabenzoporphyrin.⁹⁰ The effect of the phenylacetylene substitution is most clearly demonstrated through comparison of the electronic spectra of the Ni(II) derivatives **2Ni**–**4Ni**, which have systematically varying numbers of substituents (Figure 3a). Within this series, the Soret and Q bands shift ~ 40 nm on going from **2Ni** to **4Ni**, suggesting to a first approximation that π -delocalization associated with the extent of alkynyl substitution is worth ~ 13 nm/alkyne. However, there is an accompanying increase in the degree of nonplanar distortion observed in the crystal structures of **2Ni**–**4Ni** with increasing alkynyl substitution (Table 3), which is clearly convolved in the observed trends in the electronic spectra (vide infra).

**Figure 3.** Electronic absorption spectra of porphyrinic eneidyne, collected in CH_2Cl_2 at 25 °C: (a) **2Ni** (—), **3Ni** (···), **4Ni** (---); (b) **4Zn** (---), **4Mg** (—), **4Cu** (···).

Comparison of the electronic spectra of the series of octaalkynylporphyrin derivatives with differing central cations reveals a sequential red shift of the Soret absorption band energy in the order $\text{Mg} < \text{H}_2 < \text{Zn} < \text{Cu} < \text{Ni}$ in both the solid-state (Table 4) and solution (Table 4, Figure 3b) spectra. This effect clearly does not derive from metal–porphyrin π -bonding interactions, as both Ni^{2+} and Cu^{2+} have very similar back-bonding characteristics, while the π -orbitals of both Mg^{2+} and Zn^{2+} are both energetically isolated from the porphyrin π -system. The modest electronic influence of the central metal ion on the absorption band energies is further supported by the negligible differences observed in the absorption spectra of the M^{2+}TPP and M^{2+}OEP derivatives, which show only minor shifts of the Soret band upon substitution of the central metal cation.⁵⁸ From Table 3, the magnitude of the red shifts in the electronic spectra correlates well with the degree of planarity determined from the crystallographically characterized structures. The most planar compounds **4Mg** and **4Zn** exhibit the most red-shifted Soret maxima ($\lambda_{\text{max}} = 510$ nm), while that of **4Ni** is the most blue-shifted ($\lambda_{\text{max}} = 499$ nm). These trends are also retained in solution (**4Ni**, $\lambda_{\text{max}} = 497$ nm; **4Mg**, $\lambda_{\text{max}} = 515$ nm), suggesting that the structural distortion is not crystal packing in origin. Thus, the dependence of the optical spectra of the octaalkynylporphyrin derivatives on central macrocycle substitution appears to be a direct consequence of the out-of-plane geometric distortions of the porphyrin skeleton. These observations are contrary to the commonly held,^{66,91} and significantly debated,^{65–68} view that distortions of porphyrins by definition cause red shifts in the electronic spectra. Concurrent with this work, Shelnutt et al.⁹² quan-

(91) Miura, M.; Majumder, S. A.; Hobbs, J. D.; Renner, M. W.; Furenliid, L. R.; Shelnutt, J. A. *Inorg. Chem.* **1994**, *33*, 6078–6085.(92) Haddad, R. E.; Gazeau, S.; Pecaut, J.; Marchon, J.-C.; Medforth, C. J.; Shelnutt, J. A. *J. Am. Chem. Soc.* **2003**, *125*, 1253–1268.(90) Lash, T. D. *J. Porphyrins Phthalocyanines* **2001**, *5*, 267–288.

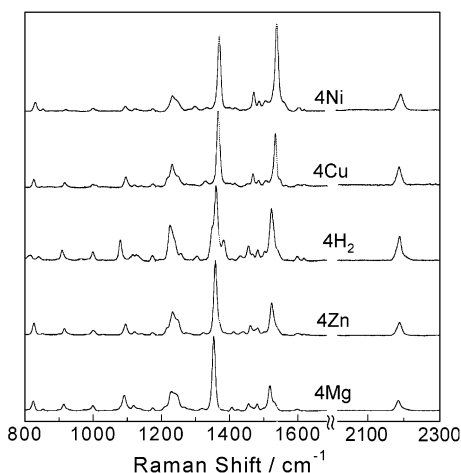


Figure 4. Solid-state resonance Raman ($\lambda = 501.7$ nm) spectra of the octaalkynylporphyrinic enediynes at 200 K (KBr).

titatively showed that out-of-plane distortions along the $2B_{1u}$ and $3B_{1u}$ normal modes can lead to red shifts in the electronic spectra of substituted porphyrins, and that seemingly small distortions along specific normal modes can contribute dramatically to electronic spectral shifts. Within the empirical correlation of the maximum red shift with planarity, the mixed ruffle/saddle character of the compounds in Table 3 leads to the possibility that small distortions along key normal modes may contribute to the observed spectral red shifts.

Resonance Raman Spectroscopy. Resonance Raman spectra ($\lambda_{\text{exc}} = 501.7$ nm) of the octaalkynyl series of compounds **4Ni**, **4H₂**, **4Zn**, **4Cu**, and **4Mg** are shown in Figure 4. Systematic shifts to lower energy of the two dominant resonance Raman vibrations at ~ 1365 and ~ 1530 cm^{-1} are observed as a function of central macrocycle substitution. Frequency shifts of the structure-sensitive Raman bands (ν_2 , ν_3 , ν_4 , ν_{10} , and ν_{19} as defined by the notation of Kyogoku and co-workers⁹³) of the core macrocycle are known to occur upon distortion from planarity.^{91,94–96} In the octaalkynyl derivatives, structural distortion derives from a decrease in the atomic core size proceeding along the series Ni^{2+} to Mg^{2+} . This effect is reflected in the X-ray structures as an increase in the average M–N bond lengths from 1.918 Å for Ni^{2+} to 2.072 Å for Mg^{2+} , as well as a decrease in the $\text{C}_\alpha\text{--N--C}_\alpha$ angle from 107.6° in **4Mg** to 106.6° in **4Ni** (Table 3). Shifts to lower energy of the ~ 1365 cm^{-1} vibration (ν_4 , pyrrole breathing mode) and the ~ 1530 cm^{-1} band (ν_3 , in-plane $\text{C}_{\text{meso}}\text{--C}_\alpha\text{--C}_\beta$)^{93–95,97} across the octaalkynyl series display a negative linear relationship ($R^2 = 0.96$ and 0.98 , respectively) when plotted relative to the $\text{C}_\alpha\text{--N--C}_\alpha$ angle, which correlates loosely with the overall degree of deviation from the mean plane.^{64,89} While devia-

tions from planarity observed in the solid state are not always retained in solution, the trends observed across the solid-state Raman spectra are conserved in spectra collected in CH_2Cl_2 solution at room temperature.

Significant resonance enhancement is also observed for the Raman vibrations at ~ 1234 and ~ 1095 cm^{-1} . Neither of these features show shifts that correlate with distortion of the porphyrin backbone. In accordance with this observation, and on the basis of their frequencies, they can be coarsely assigned as in-plane skeletal modes of the macrocycle.⁹⁴ The bands at ~ 920 , ~ 1000 , and 1600 cm^{-1} are unaffected by distortion of the porphyrin ring and demonstrate only modest resonance enhancement. The absence of these modes in the spectrum of NiOEP^{93,98} and their shift upon perdeuteration in the spectrum of NiTPP⁹⁹ both suggest that these modes are associated with the phenyl rings at the *meso*-positions.^{94,99} In the porphyrinic enediynes, these vibrational features may also have contributions from the β -phenylacetylene units as their vibrational frequencies would be nearly degenerate.

Electronic delocalization of the porphyrin $\pi\text{--}\pi^*$ excited state through the alkyne units is clearly observed via enhancement of the alkyne stretch observed in the resonance Raman spectra obtained with $\lambda_{\text{exc}} = 501.7$ nm. Minor shifts are also observed in the alkyne stretching frequencies as a function of central cation substitution. **4Ni** has the highest energy alkyne stretch at 2192 cm^{-1} , while the other derivatives are grouped tightly in the range of $2189\text{--}2186$ cm^{-1} with the order **4Cu** \approx **4H₂** \approx **4Zn** $>$ **4Mg**. These vibrational frequencies are markedly lower than those observed for simple nonconjugated, nonbenzannulated enediynes ($\nu_{\text{CC}} \approx 2230$ cm^{-1}), as well as their benzannulated counterparts with conjugated quinoline functionalities at the alkyne termini ($\nu_{\text{CC}} \approx 2209$ cm^{-1}).^{38,39,41,100} Thus, the shift of ν_{CC} to lower frequency in the porphyrinic enediynes derives from electronic delocalization of the porphyrin macrocycle through the alkynes, which leads to a decrease in the $\text{--C}\equiv\text{C--}$ bonding character and hence a decrease in the alkyne stretching frequency. The degree of delocalization and corresponding shift in the alkyne stretching frequency can be modestly altered by changing the central porphyrin cation, which produces a systematic distortion in the macrocycle structure (Table 3). Therefore, the frequency of ν_{CC} (**4Ni** $>$ **4Cu** \approx **4H₂** \approx **4Zn** $>$ **4Mg**) is weakly related to the degree of distortion of the macrocycle in the order **4Ni** $>$ **4Cu** $>$ **4H₂** $>$ **4Zn** \approx **4Mg** (Table 3).

Changes in the resonance Raman spectrum of **2Ni–4Ni** are also observed upon increasing the number of phenylacetylene substituents (Figure 5). A sequential shift of the dominant features at ~ 1370 and ~ 1530 cm^{-1} to lower energy is observed upon increasing the number of alkynyl substituents from five to eight. These are the same modes that shift to higher energy with increasing macrocycle distortion

(93) Abe, M.; Kitagawa, T.; Kyogoku, Y. *J. Chem. Phys.* **1978**, *69*, 4526–4534.

(94) Spiro, T. G. In *Physical Bioinorganic Chemistry Series: Iron Porphyrins, Part 2*; Lever, A. B. P., Gray, H. B., Eds.; Addison-Wesley: London, 1983; pp 89–159.

(95) Shelnutt, J. A.; Medforth, C. J.; Berber, M. D.; Barkigia, K. M.; Smith, K. M. *J. Am. Chem. Soc.* **1991**, *113*, 4077–4087.

(96) Piffat, C.; Melamed, D.; Spiro, T. G. *J. Phys. Chem.* **1993**, *97*, 7441–7450.

(97) Sparks, L. D.; Anderson, K. K.; Medforth, C. J.; Smith, K. M.; Shelnutt, J. A. *Inorg. Chem.* **1994**, *33*, 2297–2302.

(98) Li, X. Y.; Czernuszewicz, R. S.; Kincaid, J. R.; Su, Y. O.; Spiro, T. G. *J. Phys. Chem.* **1990**, *94*, 31–47.

(99) Li, X. Y.; Czernuszewicz, R. S.; Kincaid, J. R.; Stein, P.; Spiro, T. G. *J. Phys. Chem.* **1990**, *94*, 47–61.

(100) Kraft, B. J.; Zaleski, J. M. Unpublished results.

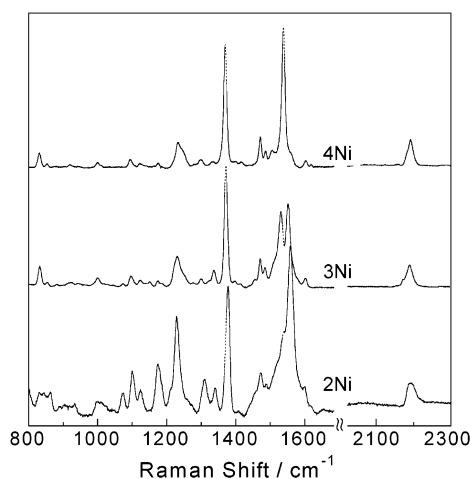


Figure 5. Resonance Raman spectra of the nickel penta-, hexa-, and octaalkynylporphyrinic enediynes collected with 457.9, 488.0, and 501.7 nm excitation, respectively. All spectra were recorded at 200 K in KBr.

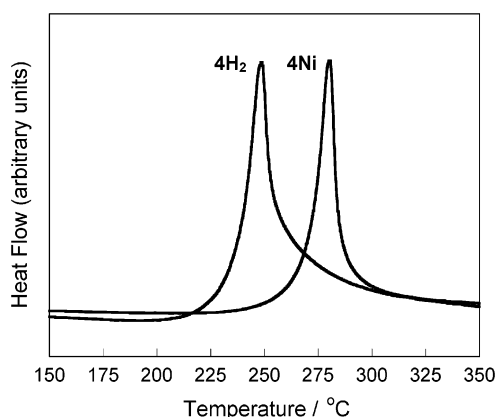


Figure 6. DSC traces for the Bergman cyclization of **4Ni** (281 °C) and **4H₂** (248 °C) within the solid state.

(Figure 5). From the crystallographic data for **2Ni–4Ni**, the degree of distortion increases with increasing substitution number. Thus, one would expect, as is well predated,^{91,94–96} that these structure-sensitive Raman bands would shift to higher energy with increasing substitution. Interestingly, the opposite trend is observed in the Raman spectra of **2Ni–4Ni** (Figure 6). From the dramatic red shifts in the optical spectra of these compounds, it is clear that there are electronic consequences to increasing the number of periphery substituents. Thus, one could conclude that both of these parameters will influence the Raman spectrum.

The observed shifts in the resonance Raman spectra of the porphyrinic enediynes would suggest there are two parameters that affect the observed frequencies of the structure-sensitive Raman bands. The first is a well-precedented geometric effect, which causes a shift of these bands to higher energy with increasing macrocycle distortion. The second is an electronic effect that results in a shift of these features to lower energy with increasing delocalization. Across the octaalkynyl series (Figures 3b and 4), there is a relatively modest blue shift in the electronic spectra, and the Raman marker bands move to higher energy with increasing macrocycle distortion. For this group, shifts in the Raman spectra appear to be dominated by the degree of geometric

Table 5. Average Alkyne Termini Separation and Bergman Cyclization Temperatures for **2–14** Determined by DSC

compd	av alkyne termini separation/Å	temp/ °C	compd	av alkyne termini separation/Å	temp/ °C
2Ni	4.09	275	4Mg	3.77	244
3Ni	3.95	261	5Ni		361
4Ni	4.00	281	5H₂		351
4Cu	3.79	247	5Zn		347
4H₂	3.82	248	5Cu		345
4Zn	3.79	249	6H₂	4.23	302

distortion. Conversely, increased substitution from **2Ni** to **4Ni** (Figures 3a and 5) leads to a pronounced red shift in the electronic spectra, and a corresponding shift in the Raman marker bands to lower frequency. Hence, π -delocalization throughout the porphyrin framework causes a shift of the marker bands to lower frequency, despite the competing effect of the geometric distortion, which in the octaalkynyl series leads to an increase in these vibrational frequencies.

Solid-State Thermal Reactivity. Differential scanning calorimetry has been shown to be an effective tool for measuring Bergman cyclization temperatures of metalloene-diyne structures in the solid state (absence of a H donor), and effectively correlating the temperature with the distance between the alkyne termini.^{51–62} Within this theme, the thermal Bergman cyclization temperatures for **2Ni–4Ni**, **4H₂**, **4Cu**, **4Zn**, **4Mg**, **5Ni**, **5Zn**, **5Cu**, and **6H₂** determined in the solid state by DSC are given in Table 5. Where applicable, the cyclization temperatures are compared to crystallographically measured alkyne termini separation distances in an effort to evaluate the dependence of reactivity upon structural differences at the porphyrin periphery. Table 3 reveals a systematic distortion of the macrocycle as a function of the numbers of alkyne substituents, and the nature of the central macrocycle cation. For **2Ni–4Ni**, the X-ray structures show only limited differences in the average alkyne termini separation (**2Ni**, 4.09 Å; **3Ni**, 3.95 Å; **4Ni**, 4.00 Å). Interestingly, the thermal Bergman cyclization temperatures (**2Ni**, 275 °C; **3Ni**, 261 °C; **4Ni**, 281 °C) loosely parallel these average distances. Since termini separation is an averaged quantity over several independent units, the fact that a measurable, albeit weak, correlation exists is significant, and therefore reflects the importance of the distance dependence to the Bergman cyclization reaction within this class of structures.

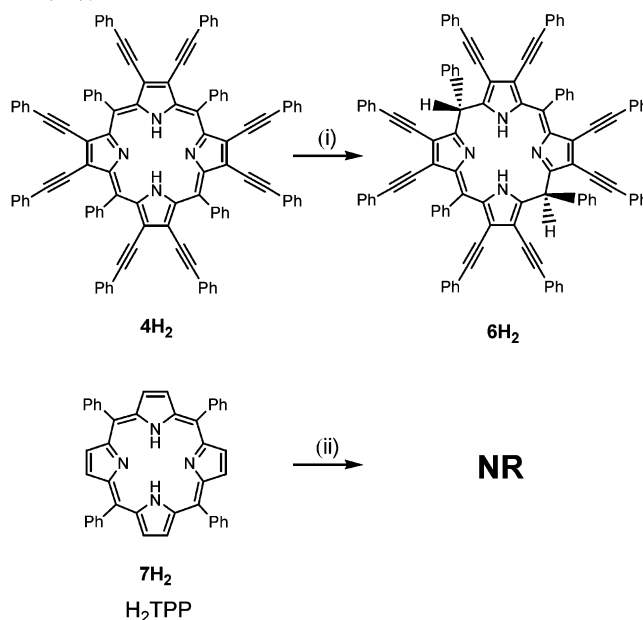
The pronounced differences in the degrees of distortion along the octaalkynyl series **4Ni**, **4H₂**, **4Cu**, **4Zn**, and **4Mg** (Table 3) generates increased variability in the average alkyne termini separation (**4Ni**, 4.00 Å; **4H₂**, 3.82 Å; **4Zn**, 3.79 Å; **4Mg**, 3.77 Å; **4Cu**, 3.79 Å; Table 5). In light of the structure/reactivity relationship in **2Ni–4Ni**, these differences would be expected to lead to enhanced variation of the Bergman cyclization temperature across the series. Indeed this is the case as the average alkyne termini separation in **4H₂** (3.82 Å) is considerably less than in **2Ni–4Ni** despite the asymmetry in the independent units (3.77 and 3.87 Å), and consequently, **4H₂** possesses a cyclization temperature that is markedly lower than those of **2Ni–4Ni** (248 °C, Figure 6). This general trend continues across **4Cu**, **4Zn**, and **4Mg** as the Bergman cyclization temperatures are all grouped very

close to that of **4H₂** (**4Zn**, 249 °C; **4Mg**, 244 °C; **4Cu**, 247 °C) but are thermally well-separated from that of the highly distorted **4Ni**. Finally, the cyclization temperatures for the (TMS)₈ analogues **5H₂**, **5Ni**, **5Zn**, and **5Cu** are considerably higher than those of their corresponding phenylacetylene counterparts (**5H₂**, 351 °C; **5Ni**, 361 °C; **5Zn**, 347 °C; **5Cu**, 345 °C). The (TMS)₈ derivatives would be expected to create significant steric hindrance and possibly electronic contributions to the activation barrier to Bergman cyclization. Since the crystal structures for these compounds were not obtained, drawing structure/reactivity relationships within this series is not appropriate. Although these correlations are not without minor inconsistencies, the overarching trend in the stability of the enediyne unit with increasing termini separation appears to hold. Perhaps more importantly, deviations in macrocycle structure and planarity can induce marked perturbations in the observed cyclization temperatures.

Thermal and Photochemical Solution Reactivity. Conjugation of the enediyne unit into the porphyrin π – π^* electronic transitions leads to fundamental questions regarding the viability for photochemical Bergman cyclization upon macrocycle-centered π – π^* excitation. Due to lifetime quenching by open d shell metalated compounds, the free-base derivative **4H₂** was photolyzed with $\lambda \geq 420$ nm light in benzene-*d*₆ using (> 100-fold) degassed 1,4-cyclohexadiene at 13 °C. Upon photolysis, the solution turns a deep red color, and a sharp singlet appears at δ 6.44 in the ¹H NMR spectrum, indicating reduction in macrocycle aromaticity. Commensurate with this new proton signal, the splitting pattern of the phenyl protons in the photoproduct ¹H NMR spectrum is dramatically altered relative to that of **4H₂**. In the ¹³C NMR spectrum, four distinct alkyne carbons are observed at δ 82.23, 83.63, 98.38, and 102.53, consistent with the decrease in symmetry of the macrocycle caused by reduction of two of the four *meso*-positions (Scheme 3). Reduction of the macrocycle was confirmed by X-ray crystallography (Figure 7, Table 6) and was also detected by measurable shifts in the electronic spectrum, as well as a significant decrease in the extinction coefficient of the final photoproduct **6H₂** (Figure 8).

The conformation of **6H₂** can be described as a rooflike structure in which the core skeleton of **6H₂** is folded along the line joining the two reduced *meso*-carbon atoms, with the two *meso*-phenyl antennae in the *syn*-conformation. Compound **6H₂** also has the lowest C _{α} –C_{*meso*}–C _{α} angles (110.13° and 111.81° for the reduced centers), which are significantly smaller than those observed for all of the phenylacetylene-substituted derivatives. This decreased angle is reflected in the N \cdots N distance of neighboring pyrroles (N1 \cdots N11 and N11 \cdots N23) which have nearest-neighbor contacts of 3.040 and 2.729 Å, respectively. These are significantly different from those observed for **4H₂** (2.967 and 2.934 Å), further illustrating the rooflike structure of **6H₂**. The reduced *meso*-carbon to *meso*-phenyl distances are 1.516 Å (C5–C41) and 1.527 Å (C18–C85), which are slightly longer than those observed in **4H₂** (1.490 and 1.512 Å), reflecting a decreased bonding interaction between these two centers. The lack of photoreactivity of **4H₂** in the absence

Scheme 3. Comparison of the Photolysis and Thermolysis of H₂P(PA)₈ and H₂TPP^a



^a Reaction conditions: (i) benzene, CHD, 420 nm/1,2,4-trichlorobenzene, CHD/IPA, 250 °C; (ii) benzene, CHD, 420 nm/1,2,4-trichlorobenzene, CHD/IPA, 250 °C.

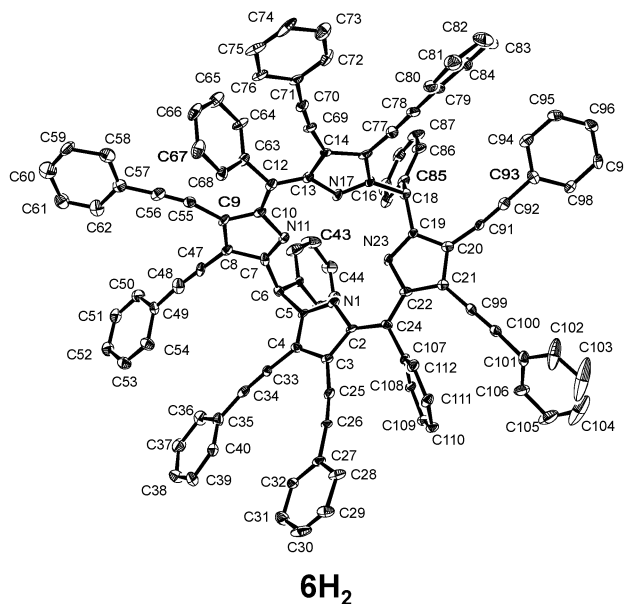


Figure 7. ORTEP of the X-ray crystal structure of **6H₂**. Thermal ellipsoids are illustrated at 50% probability.

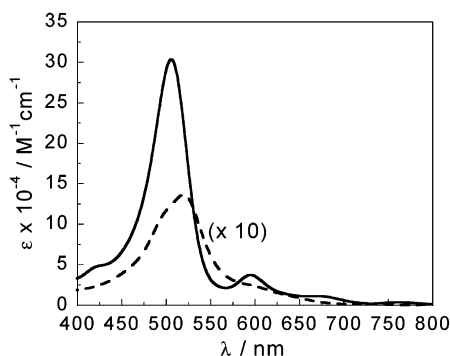
of an external H-atom donor reveals that reduction at the *meso*-positions must involve an external H-atom donor. Finally, the average alkyne termini separation is dramatically increased to 4.23 Å relative to those of the other porphyrinic enediynes (~3.8 Å, Table 5). This is reflected in a significant increase in the thermal Bergman cyclization temperature measured by DSC (302 °C, Table 5), which further supports the alkyne termini separation/cyclization temperature correlation for the octalkynyl derivatives (Table 5).

As a control, **4H₂** was thermolyzed (250 °C) anaerobically in 1,2,4-trichlorobenzene using CHD as well as 2-propanol as H-atom donors. The thermolysis reaction leads to the

Table 6. Crystallographic Data for **6H₂**

empirical formula	C ₁₀₈ H ₆₂ N ₄ ·CHCl ₃	V, Å ³	3926.4(13)
fw	1206.38	Z	2
cryst color	black	ρ_{calcd} , g/cm ³	1.531
cryst syst	monoclinic	T, K	82
space group	P2 ₁	λ , Å	0.71073
a, Å	14.962(3)	refined on the basis of	F ²
b, Å	16.981(3)	GOF	1.048
c, Å	15.520(3)	final R indices ^a	R1 = 0.115,
		[I > 2 σ (I)]	wR2 = 0.294
α , deg	90	R indices ^a (all data)	R1 = 0.166,
			wR2 = 0.326
β , deg	95.289(6)	largest diff peak and hole	0.973 and -0.568
γ , deg	90		

$$^a R1 = \sum(|F_o| - |F_c|)/\sum|F_o|. \text{ wR2} = [\sum[w(F_o^2 - F_c^2)^2]/\sum[w(F_o^2)^2]]^{1/2}.$$

**Figure 8.** Electronic absorption spectra of **4H₂** (—), and the *meso*-reduced photoproduct **6H₂** (---) collected in CH₂Cl₂ at 25 °C.

identical octasubstituted 5,15-dihydroporphyrin product **6H₂** in 67–73% yield depending upon the H-atom donor. Thus, both the photochemical and thermal reactions ultimately converge to a common chemical product, despite the vast differences in these two reaction conditions. Interestingly, neither thermolysis nor photolysis of H₂TPP (**7H₂**) under identical conditions leads to *meso*-carbon reduction (Scheme 3). This suggests that the extensive peripheral alkyne substitution may increase the electrophilicity of the *meso*-position in **4H₂** via a decrease in the redox potential (**4H₂**, $E^{+/0} = 0.56$ V, $E^{0/-} = -1.11$ V, $E^{-/2-} = -1.27$ V; **7H₂**, $E^{+/0} = 0.71$ V, $E^{0/-} = -1.58$ V, $E^{-/2-} = -1.98$ V vs Fc⁺/Fc), as well as enhance the ability of the macrocycle to stabilize a potential transient porphyrin radical upon initial H-atom addition to the double bond.

The propensity for both photochemical and thermal reduction of **4H₂** at the *meso*-carbon, and the inability to form Bergman product upon visible region chromophore excitation, generates questions regarding the fundamental pathways by which structures such as **4H₂** react. To date, spectroscopic or theoretical models describing the excited-state dynamics upon enediyne excitation are scarce,⁴⁷ and do not yet provide sufficient predictive insight into the design and corresponding reactivity of enediynes incorporated into extended chromophores. Within this context, the photochemical and thermal solution reactivity results described herein can be explained by a coarse experimental model that lends insight into the future design of chromophore–enediyne constructs for photo-Bergman cyclization. In reference to structures such as **4H₂**, excitation of a predominantly chromophore-centered π – π^* state delocalizes the excited-

state population onto the enediyne linkage via the out-of-plane π -orbitals. However, unlike simple enediynes without an adjacent π -system, the highly conjugated chromophore leads to (i) rapid internal conversion to lower-lying chromophore-centered excited states due to the overall increase in the density of states, which (ii) decreases the population of a reactive configuration that yields Bergman-cyclized product, and favors other photophysical (fluorescence, phosphorescence) or photochemical side processes. The result of these is (iii) a decrease in the lifetime of a photoinduced geometric distortion required to generate Bergman product upon electronic excitation. Thus, one approach to driving photochemical and thermal Bergman product formation in solution for a system such as **4H₂** may be reduction of the activation barrier to cyclization by a decrease in the alkyne termini separation via organic¹⁰ or inorganic^{33,37–39,41,42} ring-closing strategies, thereby channeling energy into the specific Bergman cyclization reaction coordinate. Clearly, more experimental and theoretical work is needed to properly evaluate this model; however, on the basis of the established relationship between the alkyne termini separation and Bergman cyclization thermodynamics, this concept is plausible.

Conclusion

Reaction of the appropriate 2,3,7,8,12,13,17,18-octabromo-5,10,15,20-tetraphenylporphyrin with trimethyl(phenylethynyl)tin leads to a series of substituted porphyrinic enediyne structures with varying numbers (five to eight) of alkynyl substituents. The crystal structures of several of these compounds reveal systematic ruffle, saddle, or wave distortions of the porphyrin macrocycle based on the number of alkyne substituents and the central cation. These distortions are also observed in the solid-state and solution optical spectra as a systematic red shift in the electronic transitions as a function of increasing π -delocalization and decreasing macrocycle distortion. The trend is also coarsely detected in the Raman spectra of these compounds as traditional Raman core modes, as well as the alkyne stretch, shift to lower frequency with decreasing distortion. The compounds represent a unique structural series from which trends in electronic properties of substituted porphyrins can be evaluated and compared to those previously proposed in the literature.

In addition to the influence of structure on the electronic properties of these compounds, decreasing distortion also leads to a corresponding decrease in the alkyne termini separation at the porphyrin periphery, which is reflected in a commensurate decrease in the solid-state Bergman cyclization temperatures. This trend further emphasizes the correlation between alkyne termini separation and Bergman cyclization reactivity. In solution, both π – π^* photoexcitation and thermolysis of the free-base porphyrinic enediyne in the presence of a H-atom donor lead to *meso*-carbon reduction of the macrocycle, whereas the corresponding H₂TPP compound is unreactive under identical conditions. The disparity indicates that alkyne substitution in **4H₂** activates alternate photochemical and thermal reaction pathways to

photo-Bergman cyclization. The results show that photocyclization in such extended π -structures can be challenging, and suggest that reduction in the activation barrier to Bergman cyclization by reducing the alkyne termini separation may be required to force enediyne-centered reactivity to become the dominant reaction coordinate.

Acknowledgment. The generous support of the National Institutes of Health (Grant R01 GM62541-01A1) and National Science Foundation (Grant CHE-0077942) is grate-

fully acknowledged. We also thank Dr. Maren Pink for assistance with the structural analysis and Professor Dan Mindiola for use of electrochemical equipment.

Supporting Information Available: Crystallographic data including complete tables of bond distances and angles, final fractional coordinates, and thermal parameters and ORTEP drawings of the X-ray crystal structures. This information is available free of charge via the Internet at <http://pubs.acs.org>.

IC030035A